LBL-33453
UC-414

Lawrence Berkeley Laboratory

UNIVERSITY OF CALIFORNIA

Physics Division

Radiative Corrections to the Higgs Sector of the Minimal Supersymmetric Model

D.M. Pierce
(Ph.D. Thesis)

January 1993

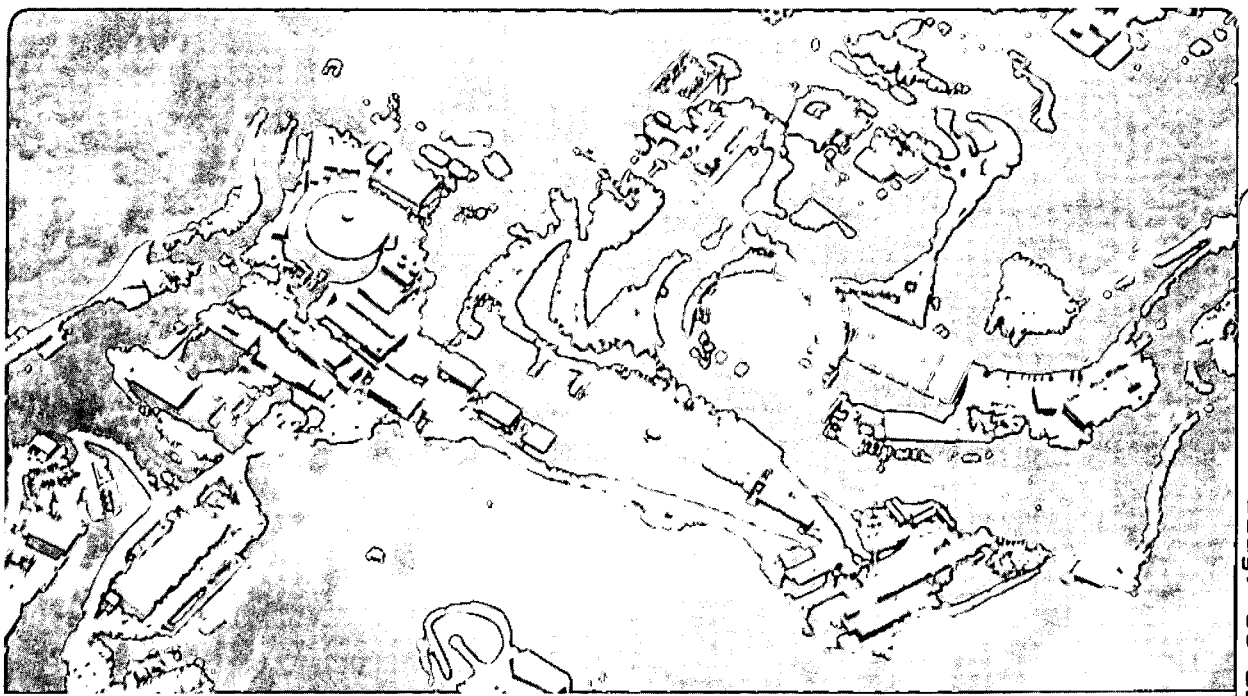

LBL-33453
Copy 1
REFERENCE COPY
Does Not
Circulate
Bldg. 50 Library.

Prepared for the U.S. Department of Energy under Contract Number DE-AC03-76SF00098

DISCLAIMER

This document was prepared as an account of work sponsored by the United States Government. While this document is believed to contain correct information, neither the United States Government nor any agency thereof, nor the Regents of the University of California, nor any of their employees, makes any warranty, express or implied, or assumes any legal responsibility for the accuracy, completeness, or usefulness of any information, apparatus, product, or process disclosed, or represents that its use would not infringe privately owned rights. Reference herein to any specific commercial product, process, or service by its trade name, trademark, manufacturer, or otherwise, does not necessarily constitute or imply its endorsement, recommendation, or favoring by the United States Government or any agency thereof, or the Regents of the University of California. The views and opinions of authors expressed herein do not necessarily state or reflect those of the United States Government or any agency thereof or the Regents of the University of California.

January 11, 1993 LBL-33453

Radiative Corrections to the Higgs Sector of the Minimal Supersymmetric Model *

Ph.D. Thesis

Damien M. Pierce

Physics Division
Lawrence Berkeley Laboratory
1 Cyclotron Road
Berkeley, California 94720

Abstract

We investigate the effect of radiative corrections on the Higgs sector of the minimal supersymmetric model (MSSM). We first consider corrections to the masses of the CP-even Higgs-bosons in the effective potential approximation. We include all sectors of the theory in the approximation that each sector is characterized by one mass scale. We demonstrate that the top-stop contribution dominates the corrections for top-quark masses above ~ 130 GeV. We than examine the decay rate of the heavy CP-even Higgs-boson $\Gamma(H \to ZZ)$. We compute radiative corrections due to virtual top- and stop-loops. We perform a Feynman diagram calculation in the on-mass-shell renormalization scheme. We find that, while the tree-level rate falls off as $1/M_H$ for large Higgs mass, the radiative corrections cause the rate to grow for sufficiently large M_H. We find that the rate can vary by two orders of magnitude when considering the effects of squark mixing. Lastly we examine the branching ratios of the heavy Higgs-boson of the MSSM. We again examine the effect of squark mixing and conclude that the squark mixing parameters must be measured in order to make precise predictions concerning the properties of the heavy Higgs-boson.

*This work was supported by the Director, Office of Energy Research, Office of High Energy and Nuclear Physics, Division of High Energy Physics of the U.S. Department of Energy under Contract DE-AC03-76SF00098.

Contents

1. Introduction 1

2. Bounds on the CP-even Higgs-boson masses 2

2.1 Introduction 2

2.2 The effective Lagrangian 6

2.3 Results 9

3. The Higgs-boson decay rate $\Gamma(H \to ZZ)$ 11

3.1 Introduction 11

3.2 Formalism for radiative corrections 13

3.3 Discussion 22

4. The branching ratios of the heavy Higgs boson 26

4.1 Introduction 26

4.2 General features 27

4.3 Squark mixing effects 30

Appendix 33

References 36

List of Figures

Figure 1(a) The heaviest possible light Higgs-boson mass at one loop level vs. the top-quark mass. The two lines in each of Figs. (a) and (b) correspond to the cases of either all light (100 GeV) SUSY scalars, all heavy (1 TeV) SUSY fermions, or vice versa. The stop mass is 1 TeV. 39

Figure 1(b) The heaviest possible light Higgs-boson mass at one loop level vs. the $\tan\beta$. 40

Figure 2(a) The lightest possible heavy Higgs-boson mass at one loop level consistent with the experimental bound $m_h \geq 41$ GeV, vs. the top-quark mass. The two lines correspond to varying all superparticle masses (except the stop mass) independently between 100 and 1000 GeV. The stop mass is 1 TeV. 41

Figure 2(b) The lightest possible heavy Higgs-boson mass at one loop level consistent with the experimental bound $m_h \geq 41$ GeV, vs. $\tan\beta$. 42

Figure 3 Excluded region of top-quark mass - $\tan\beta$ parameter space, found by requiring m_h to be greater than the current LEP limit of 41 GeV. For $m_A = 20$ and 40 GeV, the region to the right of curves is excluded. For $m_A = 60$ GeV and 1 TeV, the region below the curves is excluded. 43

Figure 4 The Higgs tadpole diagram. 44

Figure 5 The Higgs and gauge boson self energy diagrams. 44

Figure 6 The one loop $H \to ZZ$ Feynman diagrams included in our calculation. The dashed loops represent squarks, the solid loop represents quarks. 44

Figure 7 The tree level and one loop corrected decay rate $\Gamma(H \to ZZ)$ with m_t=160 GeV, and no mixing. (a) vs. M_H, for $\tan\beta$ =5; (b) vs. $\tan\beta$, with M_H=300 GeV. 45

Figure 8 The ratio of the corrected decay rate to the tree level rate vs. the top-quark mass. The parameters are the same as in Fig. 7(a), with the Higgs-boson mass set to 300 GeV and 1 TeV. 46

Figure 9 The ratio of the corrected rate including mixing to the corrected rate without mixing vs. the top squark mass $\tilde{m}_{t_1}$ as explained in the text. 47

Figure 10 The ratio of the corrected rate including mixing to the corrected rate without mixing vs. the top mixing parameter A_t, as explained in the text. The curves in fig. 10(a) stop at unphysical points in squark mixing parameter space. 48

Figure 11 The ratio of the corrected rate including mixing to the corrected rate without mixing, as explained in the text, vs. μ. The curve for $\tan\beta = 2$ stops at an unphysical point in the squark mixing parameter space. 49

Figure 12 The branching ratios of the heavy Higgs-boson for $m_t = 150$ GeV, $M_{sq} = 1$ TeV and $\tan\beta = 2$. Note that the scales in figures (a) and (b) are different. 50

Figure 13 The branching ratios of the heavy Higgs-boson for the same parameters as fig. 12, with $\tan\beta = 20$. Note that the scales in figures (a) and (b) are different. 51

Figure 14 The ratio of the heavy Higgs-boson branching ratios including squark mixing to the branching ratios without mixing, as explained in the text, vs. the squark mass parameter M_U. 52

Figure 15 The ratio of the heavy Higgs-boson branching ratios including squark mixing to the branching ratios without mixing vs. the top squark A-term parameter A_t. 53

Figure 16 The ratio of the heavy Higgs-boson branching ratios including squark mixing to the branching ratios without mixing vs. the Higgs mass parameter μ. 54

Figure 17 The vertex factors used in the Appendix. 55

Acknowledgements

I would like to thank and acknowledge the tremendous help and influence of Mary K. Gaillard. She helped me not only in her capacity as a teacher but also taught me much in her role as my advisor. Secondly I would like to express my gratitude to my friend and fellow graduate student (Dr!) Aris Papadopoulos for many hours of sometimes agonizing, but always, in the end, fruitful collaboration. I learned a great deal from him. Surmounting the many challenges that we encountered in the course of our research was often due in large part to his insight. I would like to thank Dr. Ian Hinchliffe for teaching me much about QCD. I am grateful to Anne Takezawa in the Physics Department for her gracious help and always warm sense of humor. I would like to thank Betty Moura and Luanne Neumann of the LBL Theory Group for their oft required help. I feel very fortunate to have been able to be a part of the theory group, and look forward to visiting as a postdoc. Finally, I would like to dedicate this thesis to my partner Susan Klein for her constant love and support.

1 Introduction

This decade may well mark a turning point in high energy particle physics. The standard model of particle interactions seems to describe (amazingly) all of the presently observed phenomena. Before the end of this decade, however, the next generation of colliders are due to begin collecting data which will quite probably reveal physics beyond the standard model. In this case the standard model of particle physics will have to be modified in order to accommodate this as yet undiscovered phenomena. For example, new heavy Z' bosons, possibly the relics of some symmetry larger than that of the standard model, may be found. Another possibility is the observance of quark or lepton substructure, i.e. compositeness of quarks and/or leptons. A techni-particle spectrum might be discovered, as would be expected if the electroweak symmetry breaking arises via technifermion condensation.

Many theorists expect that supersymmetry will be discovered. This expectation arises in the context of renormalizing theories with scalars as fundamental particles. In such theories (e.g. the standard model) the renormalization of the scalar mass involves quadratic divergences. These divergences, in the context of an effective field theory, are cut-off by some scale Λ which is the scale at which the low-energy theory is no longer valid. If the standard model is expected to be a valid theory until some grand unified scale or the Planck mass, then the scalar mass will naturally be of the order of this large scale, unless unnatural fine tuning is introduced. This disagreeable situation is cured in the supersymmetric theory, as the fermionic and bosonic contributions to the quadratic divergences suffer the well known exact cancellations. Thus, in a softly broken supersymmetric theory, with a scale of soft–supersymmetry breaking of $\mathcal{O}(1\text{ TeV})$, the huge hierarchy between the weak scale and the grand

unified scale or the Planck scale is stable under radiative corrections. Additionally, the scalar particles that are light at tree level remain light after including radiative effects.

Because of this improved ultraviolet behavior of supersymmetric models there has been much interest generated in examining such theories. If the world is in fact supersymmetric, a supersymmetric version of the standard model may emerge from the analysis of the data of the next generation of supercolliders. It is a natural starting point to first study the simplest supersymmetric model. In this thesis I will study radiative corrections to the minimal supersymmetric standard model (MSSM) [1, 2]. In Chapter 2 we will determine bounds on the masses of the two CP-even Higgs-bosons including radiative corrections from all sectors of the theory. We will find quite large corrections due to a large top-quark Yukawa coupling. In Chapter 3 we will study the renormalized HZZ vertex of the heavy CP-even Higgs-boson and the corresponding decay rate. This decay mode is a viable mode for detecting the heavy Higgs-boson at hadron supercolliders for some part of the parameter space. In the final chapter, Chapter 4, we discuss the renormalized branching ratios of the heavy Higgs boson. We study in detail the dependences of the branching ratios on the squark mixing parameters.

2 Bounds on the CP-even Higgs-boson masses

2.1 Introduction

In this chapter we address two questions of current phenomenological interest. In the minimal supersymmetric standard model there are two CP-even Higgs bosons.

These particles, which we refer to as h^0 and H^0 , are respectively lighter and heavier than the Z^0 boson at tree level. We utilize the effective Lagrangian formulation to determine the heaviest possible h^0 mass and the lightest possible H^0 mass in the MSSM to one loop order. These results are only logarithmically dependent on the mass of the CP-odd Higgs-boson, m_A, and all other soft parameters in the Lagrangian, such as superparticle masses and A-term parameters.

At tree level h^0 is constrained to be less massive than $M_Z|\cos 2\beta|$, where $\tan\beta = v_2/v_1$ is the ratio of vacuum expectation values of the two Higgs fields. This bound is saturated for $m_A \gg M_Z$. Similarly, H^0 satisfies $m_H \geq M_Z$ at tree level and this inequality saturates when $m_A = 0$. We calculate the leading logarithmic one loop corrections to these saturated inequalities. Corrections to the masses of the Higgs bosons have appeared in several papers [3]. This work has been further elaborated on in Ref. [4]. Corrections to the charged Higgs boson masses have been studied [5], and corrections to Higgs mass sum rules have been calculated [6, 7].

The two Higgs doublets in this model have the charge structure

$$H_1 = \begin{pmatrix} H_1^0 \\ H_1^- \end{pmatrix}, \qquad H_2 = \begin{pmatrix} H_2^+ \\ H_2^0 \end{pmatrix}, \tag{1}$$

and these acquire vacuum expectation values $\frac{1}{\sqrt{2}}\begin{pmatrix} v_1 \\ 0 \end{pmatrix}$ and $\frac{1}{\sqrt{2}}\begin{pmatrix} 0 \\ v_2 \end{pmatrix}$. We choose v_1 and v_2 to be real and positive. Writing $H_1^\circ = \frac{1}{\sqrt{2}}(S_1 + iP_1)$, $H_2^\circ = \frac{1}{\sqrt{2}}(S_2 - iP_2)$, we have the tree level potential for the fields S_1 and S_2

$$V_{tree} = \frac{1}{2}m_1^2 S_1^2 + \frac{1}{2}m_2^2 S_2^2 - m_3^2 S_1 S_2 + \frac{g^2 + g'^2}{32}(S_1^2 - S_2^2)^2. \tag{2}$$

The coefficient of the quartic term is a combination of g and g', the $SU(2)$ and $U(1)$ coupling constants, respectively. This is in contrast to the standard model where

the coefficient of the quartic term in the Higgs potential is arbitrary. The masses* of the CP-even Higgs-bosons are given by the eigenvalues of the mass matrix

$$m_{ij}^2 = \frac{\partial^2 V}{\partial S_i \partial S_j} \tag{3}$$

where V is the scalar potential. We define v_1 and v_2 to be the vacuum expectation values of H_1^0 and H_2^0 by requiring

$$\left.\frac{\partial V}{\partial S_1}\right|_{v_1,v_2} = 0 = \left.\frac{\partial V}{\partial S_2}\right|_{v_1,v_2} . \tag{4}$$

At tree level, we can use eqs. (3) and (4) to obtain the mass relation

$$m_{h,H}^2 = \frac{1}{2}\left(m_A^2 + M_Z^2 \mp \sqrt{(m_A^2 + M_Z^2)^2 - 4M_Z^2 m_A^2 \cos^2 2\beta}\right), \tag{5}$$

where $M_Z^2 = \frac{1}{4}(g'^2 + g^2)(v_1^2 + v_2^2)$ and $m_A^2 = m_3^2(\tan\beta + \cot\beta)$. At one loop level the potential

$$V^{(1)} = V_{tree} + \Delta V^{(1)} \tag{6}$$

can be explicitly modified so that v_1 and v_2 receive no corrections. To do this we simply add to $\Delta V^{(1)}$ terms proportional to S_1^2 and S_2^2 by redefining the tree parameters m_1 and m_2. We have

$$V^{(1)} = V'_{tree} + \Delta V^{(1)'}, \tag{7}$$

$$\Delta V^{(1)'} = \Delta V^{(1)} + aS_1^2 + bS_2^2, \tag{8}$$

where the primes indicate the redefined potentials. We determine a and b by requiring

$$\left.\frac{\partial \Delta V^{(1)'}}{\partial S_1}\right|_{v_1,v_2} = 0 = \left.\frac{\partial \Delta V^{(1)'}}{\partial S_2}\right|_{v_1,v_2} . \tag{9}$$

*The physical mass is given by the pole of the propagator. The inverse propagator is $p^2 - m_{tree}^2 + \Pi(p^2)$, where $\Pi(p^2)$ is the self energy. At one loop $V^{(1)''} = m_{tree}^2 - \Pi(0)$, while the physical mass squared is $m_{tree}^2 - \Pi(m_{tree}^2)$. However, we consider cases where $m_{tree} \simeq M_Z$, so we expect the difference $\Pi(m_{tree}^2) - \Pi(0)$ between $V^{(1)''}$ and the physical mass to be small.

Hence,

$$a = -\frac{1}{2v_1}\frac{\partial \Delta V^{(1)}}{\partial S_1}\bigg|_{v_1,v_2}, \qquad b = -\frac{1}{2v_2}\frac{\partial \Delta V^{(1)}}{\partial S_2}\bigg|_{v_1,v_2}, \tag{10}$$

and the correction to the mass matrix is given by

$$\Delta m^2_{ij} = \frac{\partial^2 \Delta V^{(1)}}{\partial S_i \partial S_j}\bigg|_{v_1,v_2} - \delta_{i1}\delta_{j1}\frac{1}{v_1}\frac{\partial \Delta V^{(1)}}{\partial S_1}\bigg|_{v_1,v_2} - \delta_{i2}\delta_{j2}\frac{1}{v_2}\frac{\partial \Delta V^{(1)}}{\partial S_2}\bigg|_{v_1,v_2}. \tag{11}$$

The one loop potential has three contributions,

$$\Delta V^{(1)} = \Delta V^{(1)}_{eff\ pot} + \Delta V^{(1)}_{\substack{gauge\\ renorm}} + \Delta V^{(1)}_{\substack{wave\\ function}}, \tag{12}$$

and we discuss these three contributions in turn. We should remark on the renormalizations in eq. (12). By computing the three terms above of we are including the contributions of the effective Lagrangian. Some authors utilize just the effective potential in calculations and do not explicitly include wave function and gauge coupling renormalization in their procedure. Instead, they introduce a renormalization scale which mimics the effect of including these renormalizations. We note that only by explicitly including these renormalizations do we find the correct threshold behavior. In particular, the arguments of the logarithms are ratios of particle masses; there are no other scales introduced. In the present case, the difference between these two procedures is numerically unimportant. As a simplification, we keep only leading logarithms whose argument is the ratio of a SUSY-particle mass to a weak scale mass. The only terms we ignore which may be important are logarithms whose argument is the ratio of the two stop masses. However, in a large class of MSSM mass spectrum scenarios the two stops are not expected to be highly nondegenerate, so that in these cases we are justified in not including these terms.

2.2 The effective Lagrangian

We now calculate the three terms in eq. (12). The first correction, $\Delta V^{(1)}_{eff\ pot}$, is due to the one loop effective potential [8],

$$\Delta V^{(1)}_{eff\ pot} = \frac{1}{64\pi^2} Str\mathcal{M}^4 \ln \frac{\mathcal{M}^2}{\Lambda^2}, \tag{13}$$

where Λ is an ultraviolet cutoff and $\mathcal{M}^2$ is the field dependent squared mass matrix for all of the spin 0, 1/2, and spin 1 particles in the model. The supertrace is defined as usual for any function f by $Strf(\mathcal{M}^2) = \sum_i (-1)^{2J_i}(2J_i+1)f(m_i^2)$ where m_i^2 is the i'th squared mass eigenvalue of the mass matrix $\mathcal{M}^2$, for a particle of spin J_i.

As we are only interested in the logarithmic corrections, we do not differentiate the logarithms in $\Delta V^{(1)}_{eff\ pot}$. Hence, we can evaluate them at the vacuum. Expanding $\Delta V^{(1)}_{eff\ pot}$ in powers of S_1 and S_2, we see from eq. (11) that all terms proportional to S_1^2 and S_2^2 do not contribute to Δm^2. Additionally, terms proportional to $S_1 S_2$ can be absorbed into a redefinition of the tree parameter m_3. This procedure leaves terms proportional to S_1^4, S_2^4 and $S_1^2 S_2^2$. It is then straightforward to determine $\Delta V^{(1)}_{eff\ pot}$ by calculating the mass matrices for all of the particles in the MSSM. We obtain the contribution to the mass matrix

$$\Delta m^2_{eff\ pot} =$$

$$\frac{3g^2 m_t^2}{8\pi^2 M_W^2}\left\{\frac{m_t^2}{\sin^2\beta}\ln\left(\frac{m_{\tilde{t}}^2}{m_t^2}\right)\begin{pmatrix}0 & 0\\ 0 & 1\end{pmatrix} + \frac{M_Z^2}{4}\ln\left(\frac{m_{\tilde{t}}^2}{\Lambda^2}\right)\begin{pmatrix}0 & \cot\beta\\ \cot\beta & -2\end{pmatrix}\right\}$$

$$+\frac{g^2 M_Z^4 \sin 2\beta}{32\pi^2 M_W^2}\left(2s_w^4 - 4s_w^2 + 3\right)\left\{\ln\left(\frac{M_H^2}{M_{1/2}^2}\right) + 3\ln\left(\frac{M_Z^2}{M_{1/2}^2}\right)\right\}\begin{pmatrix}0 & 1\\ 1 & 0\end{pmatrix} \tag{14}$$

$$+\frac{1}{64\pi^2}\left\{2\left(g'^4 + \frac{3}{2}g'^2 g^2 + g^4\right)\ln\left(\frac{M_H^2}{\Lambda^2}\right) - 2\left(g'^4 + 2g'^2 g^2 + 5g^4\right)\ln\left(\frac{M_{1/2}^2}{\Lambda^2}\right)\right.$$

$$+\frac{3}{2}\left(g'^4+2g'^2g^2+3g^4\right)\ln\left(\frac{M_Z^2}{\Lambda^2}\right)+\left(\frac{103}{12}g'^4+\frac{21}{4}g^4\right)\ln\left(\frac{M_{\tilde{Q}}^2}{\Lambda^2}\right)$$

$$+\left(\frac{17}{12}g'^4+\frac{3}{4}g^4\right)\ln\left(\frac{m_{\tilde{t}}^2}{\Lambda^2}\right)\Bigg\}\begin{pmatrix} v_1^2 & -v_1v_2 \\ -v_1v_2 & v_2^2 \end{pmatrix},$$

where $s_W = \sin\theta_W$. We write a mass $M_{1/2}$ for the higgsinos and gauginos, a mass $M_{\tilde{Q}}$ for the squarks and sleptons (except the stop mass $m_{\tilde{t}}$) and a mass M_H for the Higgs-bosons. While the superparticle masses are not degenerate in this manner, we can use these masses to estimate the effect of nondegeneracies and mixing as explained in Section 2.3.

The second contribution from the effective Lagrangian in eq. (12), $\Delta V^{(1)}_{\substack{gauge\\renorm}}$, is due to gauge coupling renormalization. We must include this contribution to renormalize the mass of the Z^0. The part of the tree potential which depends on the gauge couplings is the quartic piece

$$V_{tree}^{quartic} = \frac{1}{32}(g^2+g'^2)(S_1^2-S_2^2)^2. \tag{15}$$

We relate the renormalized coupling g_R to the unrenormalized coupling g_U through the relation $g_R = g_U - \Delta g$. Writing the tree potential in terms of the renormalized couplings gives a contribution to the potential

$$\Delta V_{\substack{gauge\\renorm}} = \frac{1}{16}(g\Delta g + g'\Delta g')(S_1^2-S_2^2)^2 \tag{16}$$

and hence (from eq. (11)) a contribution to the mass matrix

$$\Delta m^2_{\substack{gauge\\renorm}} = \frac{g\Delta g + g'\Delta g'}{2}\begin{pmatrix} v_1^2 & -v_1v_2 \\ -v_1v_2 & v_2^2 \end{pmatrix}. \tag{17}$$

We obtain the MSSM renormalizations of the gauge couplings [9]

$$\Delta g' = \frac{g'^3}{32\pi^2}\left\{\frac{17}{36}\left[\ln\left(\frac{\Lambda^2}{m_{\tilde{t}}^2}\right) + 2\ln\left(\frac{\Lambda^2}{m_t^2}\right)\right]\right.$$

$$\left. + \frac{103}{36}\left[\ln\left(\frac{\Lambda^2}{M_{\tilde{Q}}^2}\right) + 2\ln\left(\frac{\Lambda^2}{M_Z^2}\right)\right] + \frac{1}{3}\left[\ln\left(\frac{\Lambda^2}{M_H^2}\right) + 2\ln\left(\frac{\Lambda^2}{M_{1/2}^2}\right)\right]\right\},$$

$$\Delta g = \frac{g^3}{32\pi^2}\left\{\frac{1}{4}\left[\ln\left(\frac{\Lambda^2}{m_{\tilde{t}}^2}\right) + 2\ln\left(\frac{\Lambda^2}{m_t^2}\right)\right]\right.$$

$$\left. + \frac{7}{4}\ln\left(\frac{\Lambda^2}{M_{\tilde{Q}}^2}\right) + \frac{1}{3}\ln\left(\frac{\Lambda^2}{M_H^2}\right) + 2\ln\left(\frac{\Lambda^2}{M_{1/2}^2}\right) - \frac{23}{6}\ln\left(\frac{\Lambda^2}{M_Z^2}\right)\right\}. \tag{18}$$

The third correction in eq. (12), $\Delta V^{(1)}_{\substack{wave\\function}}$, arises due to wave function renormalization. Renormalizing the fields via $H_{iR} = Z_i^{-\frac{1}{2}} H_{iU}$, $(i = 1,2)$, where H_U denotes an unrenormalized field and H_R denotes a renormalized one, we get a correction to the potential†

$$\Delta V_{\substack{wave\\function}} = \frac{g^2 + g'^2}{16}(S_1^2 - S_2^2)(\Delta Z_1 S_1^2 - \Delta Z_2 S_2^2) \tag{19}$$

where the fields are renormalized and $Z_i = 1 + \Delta Z_i$. As the field H_2 couples to the top-quark, it receives an additional renormalization compared with H_1. We have the MSSM wave function renormalization [9]

$$\Delta Z_1 = \frac{3g^2 + g'^2}{16\pi^2}\left[\frac{1}{4}\ln\left(\frac{\Lambda^2}{M_H^2}\right) - \frac{1}{2}\ln\left(\frac{\Lambda^2}{M_{1/2}^2}\right) + \frac{1}{2}\ln\left(\frac{\Lambda^2}{M_Z^2}\right)\right],$$

$$\Delta Z_2 = \Delta Z_1 - \frac{3}{16\pi^2}\lambda_t^2 \ln\left(\frac{\Lambda^2}{m_t^2}\right), \tag{20}$$

where λ_t is the top-quark Yukawa coupling (we neglect the others) and the top-quark mass given by $m_t = \lambda_t v_2/\sqrt{2}$. This gives a correction to the mass matrix

†We only need to consider the quartic part of the potential here as well, since the terms proportional to S_1^2 and S_2^2 do not contribute to Δm^2 and terms proportional to $S_1 S_2$ can be absorbed by the tree parameter m_3.

$$\Delta m^2_{\substack{wave\\function}} =$$

$$\frac{g^2+g'^2}{64\pi^2}\left\{\left(3g^2+g'^2\right)\left[\frac{1}{2}\ln\left(\frac{\Lambda^2}{M_H^2}\right)-\ln\left(\frac{\Lambda^2}{M_{1/2}^2}\right)+\ln\left(\frac{\Lambda^2}{M_Z^2}\right)\right]\begin{pmatrix} v_1^2 & -v_1v_2 \\ -v_1v_2 & v_2^2\end{pmatrix}\right.$$
$$\left.+3\lambda_t^2\ln\left(\frac{\Lambda^2}{m_t^2}\right)\begin{pmatrix} 0 & v_1v_2 \\ v_1v_2 & -2v_2^2\end{pmatrix}\right\}. \tag{21}$$

2.3 Results

Combining the three corrections from the effective Lagrangian we find that the cutoff dependence cancels. We stress that we must include all three of these contributions in order to have a physical, finite result. The logarithmic corrections to the CP-even Higgs-boson mass matrix are

$$\Delta m_{11}^2 = \cos^2\beta\left(\frac{g^2M_Z^4}{96\pi^2M_W^2}\right)\left[\left(1+4s_w^2+2s_w^4\right)\ln\left(\frac{M_H^2}{M_{1/2}^2}\right)\right. \tag{22}$$
$$+\left(53-112s_w^2+62s_w^4\right)\ln\left(\frac{M_Z^2}{M_{1/2}^2}\right)+\left(21-42s_w^2+\frac{166}{3}s_w^4\right)\ln\left(\frac{M_{\tilde{Q}}^2}{M_Z^2}\right)$$
$$\left.+\left(3-6s_w^2+\frac{26}{3}s_w^4\right)\ln\left(\frac{m_{\tilde{t}}^2}{m_t^2}\right)\right]$$

$$\Delta m_{12}^2 = \sin\beta\cos\beta\left(\frac{g^2M_Z^4}{96\pi^2M_W^2}\right)\left[\left(17-28s_w^2+10s_w^4\right)\ln\left(\frac{M_H^2}{M_{1/2}^2}\right)\right.$$
$$+(1+40s_w^2-26s_w^4)\ln\left(\frac{M_Z^2}{M_{1/2}^2}\right)-(21-42s_w^2+\frac{166}{3}s_w^4)\ln\left(\frac{M_{\tilde{Q}}^2}{M_Z^2}\right) \tag{23}$$
$$\left.+\left(\frac{9m_t^2}{M_Z^2\sin^2\beta}-3+6s_w^2-\frac{26}{3}s_w^4\right)\ln\left(\frac{m_{\tilde{t}}^2}{m_t^2}\right)\right]$$

$$\Delta m_{22}^2 = \left(\frac{3g^2M_Z^4}{16\pi^2M_W^2}\right)\left[\frac{2m_t^4}{M_Z^4\sin^2\beta}-\frac{m_t^2}{M_Z^2}\right]\ln\left(\frac{m_{\tilde{t}}^2}{m_t^2}\right)+\tan^2\beta\Delta m_{11}^2. \tag{24}$$

In order to take into account all possible superparticle masses we vary the common mass parameters $M_{1/2}$, $M_{\tilde{Q}}$ and M_H appearing in our formulas from 0.1

to 1 TeV. The extrema of this variation corresponds (either exactly or very nearly) to the case where the SUSY fermions are light and the SUSY scalars are heavy, or vice versa. The variation in our results represents the theoretical uncertainty due to the lack of information on the superparticle spectrum. In keeping with the effective potential approximation, we must have some large logarithms in order for our results to be trustworthy. In particular, our result is not trustworthy for cases where the top-quark can give a large contribution to the mass, and $m_{\tilde{t}} \simeq m_t$, i.e. for cases where the logarithm multiplying the top contribution becomes small. Hence, we always set the stop mass to 1 TeV and neglect stop mixing.

In figures 1(a) and (b) we plot the heaviest possible h^0 mass as a function of the top-quark mass and $\tan\beta$, respectively. Hence we set m_A equal to 1 TeV. The two curves in the plots correspond to the cases of light SUSY scalars and heavy SUSY fermions, or vice versa. These two cases correspond to the maximal variation of the light higgs mass when allowing each SUSY mass to vary independently between 100 and 1000 GeV. We find that the uncertainty in the superparticle spectrum typically gives us an uncertainty of 3 to 5 GeV in the mass of the Higgs-bosons. The difference in the mass for $\tan\beta = 10$ and $\tan\beta = \infty$ is less than a few percent. If the stop mass is less than 1 TeV the light Higgs-boson becomes lighter than shown in Figs. 1.

At tree level the lightest possible value of the heavy Higgs-boson mass is M_Z and this occurs when $m_A = 0$. At one loop level, however, if $m_A = 0$ and if $\tan\beta$ is near 1 we find that the light Higgs-boson can become lighter than the current experimental lower bound [10] of 41 GeV. Hence we should increase the parameter[‡] m_A until the mass of the light Higgs reaches this lower bound. We can then use

[‡] m_A does not correspond to the mass of the CP-odd Higgs-boson at one loop level, as it does at tree level. However, in the limit of no squark mixing the difference is small [4].

this value of m_A to evaluate the mass of the heavy Higgs-boson. In figures 2(a) and (b) we plot the lightest possible heavy Higgs-boson mass consistent with the bound on the light Higgs-boson. The two curves in the plots show the maximal variation of the heavy Higgs-boson mass while letting all SUSY particle masses to vary independently between 100 and 1000 GeV. At tree level for $\tan\beta = 1$ the light Higgs-boson is massless, independent of m_A. At one loop level, if $m_t \lesssim 100$ GeV, the top quark contribution is not big enough to increase the mass of the light Higgs boson above the experimental bound. Hence, we see in fig. 2(a) with m_t below around 100 GeV and $\tan\beta = 1$ that $m_H \gg M_Z$. Similarly in fig. 2(b) we see for the $m_t = 90$ GeV curve that we have no lower bound on the heavy Higgs-boson mass for values of $\tan\beta \lesssim 1.5$. In figure 3 we show the excluded region in the $\tan\beta - m_t$ plane for various values of m_A. Note that for small m_A a large portion of the parameter space is excluded. This is because the tree contribution to m_h is small and thus a very large m_t is needed to meet the experimental bound.

3 The Higgs-boson decay rate $\Gamma(H \to ZZ)$

3.1 Introduction

In the MSSM we need two Higgs doublets H_1 and H_2 to give masses to up and down type fermions and to assure cancellation of anomalies. The neutral Higgs spectrum consists of two *CP*-even Higgs scalar particles H and h (where $M_H > M_h$), one *CP*-odd particle A, and a Goldstone boson G which is absorbed by and gives mass to the Z boson. The Higgs sector of the MSSM is highly constrained. At tree level the Higgs-boson masses and couplings are determined by two input parameters. We

take these to be the mass of the CP-odd Higgs-boson M_A and an angle β which at tree level is given by $\tan\beta = v_2/v_1$ where v_2 and v_1 are the vacuum expectation values of the two Higgs-boson fields H_2 and H_1. The tree level masses of the CP-even Higgs-bosons are then given by

$$M^2_{H,h} = \frac{1}{2}\Big(M_A^2 + M_Z^2 \pm \sqrt{(M_A^2 + M_Z^2)^2 - 4M_Z^2 M_A^2 \cos^2(2\beta)}\Big). \tag{25}$$

The above equation implies the inequalities $M_h < M_Z$, $M_H > M_Z$ and the sum rule $M_H^2 + M_h^2 = M_Z^2 + M_A^2$.

Recently it was shown that one loop corrections involving top-quark and squark loops can significantly modify the sum rule [7] and also violate the bound $M_h < M_Z$ [11, 3, 12]. For 1 TeV squark masses we showed in the previous chapter that the correction to the light Higgs-boson mass is of the order 20 (50) GeV for a top mass of 150 (200) GeV. Corrections to the neutral Higgs-boson mass sum rule due to the gauge-Higgs and gaugino-higgsino sectors were considered earlier [6] and were found to be generically small.

In this chapter we consider corrections to the decay rate $\Gamma(H \to ZZ)$ which is relevant for the detection of the heavy Higgs-boson at a proton supercollider such as the SSC via the "gold-plated" mode $H \to ZZ \to \ell^+\ell^-\ell^+\ell^-$, where ℓ is e or μ. We confine ourselves to corrections due to third family (top and bottom) quark and squark loops. Previous work on this subject has appeared in Ref.'s [13] and [14] where the effective potential and the renormalization group methods are used. We perform a Feynman diagram calculation utilizing the on-mass-shell renormalization scheme, and present explicit analytic results. The structure of the chapter is as follows: in Section 3.2 we present our renormalization procedure and in Section 3.3 we discuss our results. In the Appendix we present the necessary explicit formulas.

3.2 Formalism for radiative corrections

Due to the presence of mixing in the *CP*-even and *CP*-odd sectors the renormalization of the Higgs sector of the MSSM presents a few complications when compared to the standard model. Therefore, in this section we present in detail our renormalization procedure. We follow the approach of Aoki *et. al.* [15] adapted to the MSSM.

The Higgs potential in the MSSM is

$$V = \tfrac{g^2+g'^2}{8}\left(H_1^{i*}H_1^i - H_2^{i*}H_2^i\right)^2 + \tfrac{g'^2}{2}|H_1^{*i}H_2^i|^2 \tag{26}$$

$$+(m_1^2+\mu^2)H_1^{i*}H_1^i + (m_2^2+\mu^2)H_2^{i*}H_2^i - \left(m_3^2\epsilon_{ij}H_1^iH_2^j + h.c.\right),$$

where $g(g')$ is the $SU(2)_L(U(1)_Y)$ gauge coupling, the m_i's, (i = 1,2,3) are the soft supersymmetry breaking Higgs sector mass parameters, and μ is the supersymmetric Higgs mass parameter. We can absorb μ^2 in Eq. (26) by redefining $m_1^2+\mu^2 \to m_1^2$ and similarly for m_2^2. H_1 and H_2 are given in terms of the shifted (but unrotated) fields by

$$H_1 = \frac{1}{\sqrt{2}}\begin{pmatrix} v_1 + S_1 - iP_1 \\ \sqrt{2}H_- \end{pmatrix}, \qquad H_2 = \frac{1}{\sqrt{2}}\begin{pmatrix} \sqrt{2}H_+ \\ v_2 + S_2 + iP_2 \end{pmatrix}.$$

In order to discuss the tadpole and mixing structure of the theory we need the terms that are linear and quadratic in S_1, S_2 and quadratic in P_1, P_2. These are given by

$$\begin{aligned} V_s = &\left(\frac{g^2+g'^2}{8}(v_1^2-v_2^2)v_1 + m_1^2v_1 - m_3^2v_2\right)S_1 \\ &+\left(\frac{g^2+g'^2}{8}(v_2^2-v_1^2)v_2 + m_2^2v_2 - m_3^2v_1\right)S_2 \\ &+\left(\frac{g^2+g'^2}{16}(3v_1^2-v_2^2)+\frac{m_1^2}{2}\right)S_1^2 + \left(\frac{g^2+g'^2}{16}(3v_2^2-v_1^2)+\frac{m_2^2}{2}\right)S_2^2 \\ &-\left(\frac{g^2+g'^2}{4}v_1v_2 + m_3^2\right)S_1S_2 \end{aligned} \tag{27}$$

$$V_p = \left(\frac{g^2+g'^2}{16}(v_1^2 - v_2^2) + \frac{m_1^2}{2}\right) P_1^2$$
$$+ \left(\frac{g^2+g'^2}{16}(v_2^2 - v_1^2) + \frac{m_2^2}{2}\right) P_2^2 - m_3^2 P_1 P_2. \tag{28}$$

We now define the coefficients of S_1 and S_2 in Eq. (27) to be

$$T_1 = \tfrac{g^2+g'^2}{8}(v_1^2 - v_2^2)v_1 + m_1^2 v_1 - m_3^2 v_2 \tag{29}$$

$$T_2 = \tfrac{g^2+g'^2}{8}(v_2^2 - v_1^2)v_2 + m_2^2 v_2 - m_3^2 v_1. \tag{30}$$

Eliminating m_1^2, m_2^2 in favor of T_1, T_2 from Eqs. (29,30) and substituting back in Eqs. (27,28) we obtain, using a matrix notation

$$V_s = (S_1 \quad S_2)\begin{pmatrix} T_1 \\ T_2 \end{pmatrix} + \tfrac{1}{2}(S_1 \quad S_2)\begin{pmatrix} \frac{T_1}{v_1} & 0 \\ 0 & \frac{T_2}{v_2} \end{pmatrix}\begin{pmatrix} S_1 \\ S_2 \end{pmatrix} \tag{31}$$
$$+\tfrac{1}{2}(S_1 \quad S_2)\begin{pmatrix} \frac{g^2+g'^2}{4}v_1^2 + m_3^2\frac{v_2}{v_1} & -\frac{g^2+g'^2}{4}v_1 v_2 - m_3^2 \\ -\frac{g^2+g'^2}{4}v_1 v_2 - m_3^2 & \frac{g^2+g'^2}{4}v_2^2 + m_3^2\frac{v_1}{v_2} \end{pmatrix}\begin{pmatrix} S_1 \\ S_2 \end{pmatrix}$$

$$V_p = \frac{1}{2}(P_1 \quad P_2)\begin{pmatrix} \frac{T_1}{v_1} & 0 \\ 0 & \frac{T_2}{v_2} \end{pmatrix}\begin{pmatrix} P_1 \\ P_2 \end{pmatrix} + \frac{1}{2}(P_1 \quad P_2)\begin{pmatrix} m_3^2\frac{v_2}{v_1} & -m_3^2 \\ -m_3^2 & m_3^2\frac{v_1}{v_2} \end{pmatrix}\begin{pmatrix} P_1 \\ P_2 \end{pmatrix}. \tag{32}$$

The next step is to introduce rotation matrices $O(\alpha)$ and $O(\beta)$ such that the part of the CP-even and CP-odd mass matrices that does not depend on T_1, T_2 is diagonalized. Specifically, by defining

$$\begin{pmatrix} S_1 \\ S_2 \end{pmatrix} = O(\alpha)\begin{pmatrix} H \\ h \end{pmatrix} = \begin{pmatrix} \cos\alpha & -\sin\alpha \\ \sin\alpha & \cos\alpha \end{pmatrix}\begin{pmatrix} H \\ h \end{pmatrix}$$

and

$$\begin{pmatrix} P_1 \\ P_2 \end{pmatrix} = O(\beta)\begin{pmatrix} G \\ A \end{pmatrix} = \begin{pmatrix} \cos\beta & -\sin\beta \\ \sin\beta & \cos\beta \end{pmatrix}\begin{pmatrix} G \\ A \end{pmatrix}$$

we find that

$$V_s = (H \quad h)\begin{pmatrix} T_H \\ T_h \end{pmatrix} + \tfrac{1}{2}(H \;.\; h)O(-\alpha)\begin{pmatrix} \frac{T_1}{v_1} & 0 \\ 0 & \frac{T_2}{v_2} \end{pmatrix} O(\alpha)\begin{pmatrix} H \\ h \end{pmatrix}$$
$$+\tfrac{1}{2}(H \quad h)\begin{pmatrix} M_H^2 & 0 \\ 0 & M_h^2 \end{pmatrix}\begin{pmatrix} H \\ h \end{pmatrix} \tag{33}$$

$$V_p = \frac{1}{2}(G \quad A)O(-\beta)\begin{pmatrix} \frac{T_1}{v_1} & 0 \\ 0 & \frac{T_2}{v_2} \end{pmatrix} O(\beta)\begin{pmatrix} G \\ A \end{pmatrix} + \frac{1}{2}(G \quad A)\begin{pmatrix} 0 & 0 \\ 0 & M_A^2 \end{pmatrix}\begin{pmatrix} G \\ A \end{pmatrix}. \quad (34)$$

Here we have defined

$$\begin{pmatrix} T_1 \\ T_2 \end{pmatrix} = O(\alpha)\begin{pmatrix} T_H \\ T_h \end{pmatrix}.$$

The parameters β, α, M_H, M_h and M_A are related to the original fundamental parameters v_1, v_2 and m_3^2 by the following formulas

$$\tan\beta = \frac{v_2}{v_1}, \quad M_A^2 = m_3^2(\tan\beta + \cot\beta), \quad \tan 2\alpha = \frac{M_A^2 + M_Z^2}{M_A^2 - M_Z^2}\tan 2\beta, \quad (35)$$

as well as Eq. (25). Here we used $M_Z^2 = \frac{g^2+g'^2}{4}(v_1^2 + v_2^2)$. Carrying out the remaining matrix multiplications involving the tadpole contributions to the mass matrices we obtain the final result

$$V_s = HT_H + hT_h + \frac{1}{2}(H \quad h)\begin{pmatrix} M_H^2 + b_{HH} & b_{Hh} \\ b_{Hh} & M_h^2 + b_{hh} \end{pmatrix}\begin{pmatrix} H \\ h \end{pmatrix} \quad (36)$$

$$V_p = \frac{1}{2}(G \quad A)\begin{pmatrix} b_{GG} & b_{GA} \\ b_{GA} & M_A^2 + b_{AA} \end{pmatrix}\begin{pmatrix} G \\ A \end{pmatrix} \quad (37)$$

with

$$b_{HH} = \frac{2}{v\sin 2\beta}\left(T_H(\cos^3\alpha\sin\beta + \sin^3\alpha\cos\beta) + T_h\sin\alpha\cos\alpha\sin(\alpha-\beta)\right)$$

$$b_{Hh} = \frac{\sin 2\alpha}{v\sin 2\beta}\left(T_H\sin(\alpha-\beta) + T_h\cos(\alpha-\beta)\right) \quad (38)$$

$$b_{hh} = \frac{2}{v\sin 2\beta}\left(T_H\cos\alpha\sin\alpha\cos(\alpha-\beta) + T_h(\cos^3\alpha\cos\beta - \sin^3\alpha\sin\beta)\right)$$

and

$$b_{GG} = \frac{1}{v}\left(T_H\cos(\alpha-\beta) - T_h\sin(\alpha-\beta)\right)$$

$$b_{GA} = \frac{1}{v}\left(T_H\sin(\alpha-\beta) + T_h\cos(\alpha-\beta)\right) \quad (39)$$

$$b_{AA} = \frac{2}{v\sin 2\beta}\left(T_H(\sin^3\beta\cos\alpha + \cos^3\beta\sin\alpha) + T_h(\cos^3\beta\cos\alpha - \sin^3\beta\sin\alpha)\right)$$

The terms linear in H and h are to be thought of as counterterms for the tadpoles. To each order in the loop expansion we require that the total tadpole contribution vanishes. At tree level this implies $-iT_H = 0 = -iT_h$. This then gives the conventional tree level masses. At one loop $-iT_H$ ($-iT_h$) must cancel the one loop H (h) tadpole diagrams $i\tau_H$ ($i\tau_h$) (fig. 4). These conditions determine T_H and T_h and Eqs. (36-39) determine their contribution to the one loop mass matrices.

Taking as renormalized inputs $\tan\beta$ and M_A we calculate the physical masses M_H, M_h and the decay rate $\Gamma(H \to ZZ)$ at one loop. It follows that the measurement of any two of the physical quantities M_A, M_H, M_h and $\Gamma(H \to ZZ)$ will allow us to make a prediction for the other two. We stress that β is only to be viewed as a useful parametrization of physical observables. Since by itself β has no physical meaning we can renormalize it in any suitably convenient way. We explain our renormalization prescription for β below.

From this point on we adopt the following notation conventions: a quantity such as a field, coupling, or mass with a subscript 0 indicates a bare quantity, quantities which are functions of the (renormalized) input parameters have a subscript r, and renormalized fields and physical observables such as the pole of a propagator do not have subscripts. The bare tree Lagrangian contains

$$\mathcal{L} \supset \tfrac{1}{2}\partial_\mu H_0 \partial^\mu H_0 + \tfrac{1}{2}\partial_\mu h_0 \partial^\mu h_0 \tag{40}$$

$$-\tfrac{1}{2}(M_{H_0}^2 + b_{HH})H_0^2 - \tfrac{1}{2}(M_{h_0}^2 + b_{hh})h_0^2 - b_{Hh}H_0 h_0$$

where $M_{H_0}^2$ and $M_{h_0}^2$ are taken to be functions of M_{A_0}, β_0 and M_{Z_0} as given by equation (25). We now write the bare parameters in terms of renormalized parameters

and shifts

$$\beta_0 = \beta + \delta\beta, \quad M_{A_0}^2 = M_A^2 + \delta M_A^2, \quad M_{Z_0}^2 = M_Z^2 + \delta M_Z^2 \tag{41}$$

and also introduce wave function renormalization

$$H_0 = Z_{HH}^{\frac{1}{2}} H + Z_{Hh}^{\frac{1}{2}} h, \qquad h_0 = Z_{hh}^{\frac{1}{2}} h + Z_{hH}^{\frac{1}{2}} H. \tag{42}$$

Note that $Z_{HH}^{\frac{1}{2}} = 1 + \mathcal{O}(\alpha)$, $Z_{hh}^{\frac{1}{2}} = 1 + \mathcal{O}(\alpha)$ while $Z_{Hh}^{\frac{1}{2}}$, $Z_{hH}^{\frac{1}{2}}$, b_{HH}, b_{Hh}, and b_{hh} are all $\mathcal{O}(\alpha)$. Substituting equations (41) and (42) into (40) we obtain the one loop renormalized two-point functions

$$\begin{aligned} i\Gamma_{HH}(p^2) &= (Z_{HH}^{\frac{1}{2}})^2 (p^2 - M_{H_r}^2) - \frac{\partial M_{H_r}^2}{\partial x_i}\delta x_i - b_{HH} + \Pi_{HH}(p^2) \\ i\Gamma_{hh}(p^2) &= (Z_{hh}^{\frac{1}{2}})^2 (p^2 - M_{h_r}^2) - \frac{\partial M_{h_r}^2}{\partial x_i}\delta x_i - b_{hh} + \Pi_{hh}(p^2) \\ i\Gamma_{Hh}(p^2) &= Z_{Hh}^{\frac{1}{2}} (p^2 - M_{H_r}^2) + Z_{hH}^{\frac{1}{2}} (p^2 - M_{h_r}^2) - b_{Hh} + \Pi_{Hh}(p^2), \end{aligned} \tag{43}$$

where $x_i = M_A^2$, M_Z^2, β and the Π's are the scalar self-energies (fig. 5). The on-shell renormalization conditions are [15]

$$\begin{aligned} \mathrm{Re}\left(i\Gamma_{HH}(M_H^2)\right) = \mathrm{Re}\left(i\Gamma_{Hh}(M_h^2)\right) = \mathrm{Re}\left(i\Gamma_{Hh}(M_H^2)\right) = \mathrm{Re}\left(i\Gamma_{hh}(M_h^2)\right) = 0 \\ \mathrm{Re}\left(i\left.\frac{\partial \Gamma_{HH}}{\partial p^2}\right|_{p^2=M_H^2}\right) = 1 = \mathrm{Re}\left(i\left.\frac{\partial \Gamma_{hh}}{\partial p^2}\right|_{p^2=M_h^2}\right) \end{aligned} \tag{44}$$

The notation Re denotes the real part. Here M_H and M_h are the physical masses of H and h. Making the definitions $\delta M_H^2 = \mathrm{Re}\,\Pi_{HH}(M_{H_r}^2) - b_{HH}$ and similarly for δM_h^2, we obtain from Eqs. (43) and (44)

$$M_H^2 = M_{H_r}^2 + \frac{\partial M_{H_r}^2}{\partial x_{ir}}\delta x_i - \delta M_H^2 \tag{45}$$

$$M_h^2 = M_{h_r}^2 + \frac{\partial M_{h_r}^2}{\partial x_{ir}}\delta x_i - \delta M_h^2 \tag{46}$$

$$Z_{HH}^{\frac{1}{2}} = 1 - \frac{1}{2}\mathrm{Re}\,\Pi'_{HH}(M_{H_r}^2) \tag{47}$$

$$Z_{hh}^{\frac{1}{2}} = 1 - \frac{1}{2}\mathrm{Re}\,\Pi'_{hh}(M_{h_r}^2) \tag{48}$$

$$Z_{hH}^{\frac{1}{2}} = \frac{1}{M_{H_r}^2 - M_{h_r}^2}\left(-\mathrm{Re}\,\Pi_{Hh}(M_{H_r}^2) + b_{Hh}\right) \tag{49}$$

$$Z_{Hh}^{\frac{1}{2}} = \frac{1}{M_{h_r}^2 - M_{H_r}^2}\left(-\mathrm{Re}\,\Pi_{Hh}(M_{h_r}^2) + b_{Hh}\right), \tag{50}$$

where the prime in Eqs. (47,48) indicates differentiation with respect to p^2. Note that $M_{H_r}^2$ and $M_{h_r}^2$ have the same functional form as in Eq. (25) except that they are functions of renormalized quantities. Eqs. (45,46) determine the physical *CP*-even Higgs boson masses in terms of self energies, tadpole contributions, and shifts of the inputs parameters δx_i. We now determine the shifts. The shift δM_A^2 is defined so that M_A is equal to the physical A mass. An analysis similar to that of the *CP*-even sector yields

$$\delta M_A^2 = \mathrm{Re}\,\Pi_{AA}(M_A^2) - b_{AA}. \tag{51}$$

Additionally, we find for the shift in the Z-boson mass

$$\delta M_Z^2 = \mathrm{Re}\,\Pi_{ZZ}^T(M_Z^2) \tag{52}$$

where Π_{ZZ}^T is the transverse part of the Z boson self energy, $\Pi_{ZZ}^{\mu\nu} = g^{\mu\nu}\Pi_{ZZ}^T + \frac{p^\mu p^\nu}{p^2}\Pi_{ZZ}^L$. At this point it is worth noting that if we are only interested in the sum $M_H^2 + M_h^2$ we do not need a specification for $\delta\beta$. When Eqs. (45) and (46) are added the terms proportional to $\delta\beta$ cancel leaving

$$M_H^2 + M_h^2 = M_A^2 + M_Z^2 + \mathrm{Re}\,\Pi_{AA}(M_A^2) + \mathrm{Re}\,\Pi_{ZZ}^T(M_Z^2)$$
$$-\mathrm{Re}\,\Pi_{HH}(M_H^2) - \mathrm{Re}\,\Pi_{hh}(M_h^2) + b_{HH} + b_{hh} - b_{AA} \tag{53}$$

This is just the renormalization of the neutral Higgs-boson mass sum rule and the divergences in Eq. (53) implicit in the Π's and b's cancel leaving behind a finite

correction. Since we demand that M_H and M_h are physical masses they must be individually finite. Equivalently, since $M_H^2+M_h^2$ is finite we must have that $M_H^2-M_h^2$ is also free of divergences. This latter requirement gives

$$\frac{\partial\Delta}{\partial\beta}\delta\beta+\frac{\partial\Delta}{\partial M_Z^2}\delta M_Z^2+\frac{\partial\Delta}{\partial M_A^2}\delta M_A^2-\delta M_H^2+\delta M_h^2=\text{finite} \tag{54}$$

where $\Delta=\sqrt{(M_A^2+M_Z^2)^2-4M_A^2M_Z^2\cos^2(2\beta)}$. The above equation clearly determines only the "infinite" part of $\delta\beta$. By "infinite" we mean the part that is proportional to $C_{UV}=\frac{1}{\epsilon}-\gamma+\log 4\pi$ in dimensional regularization. To fully specify $\delta\beta$ we take a $\overline{MS}$ approach and define $\delta\beta$ to be purely "infinite" so that Eq. (54) becomes

$$\frac{\partial\Delta}{\partial\beta}\delta\beta=-\left(\frac{\partial\Delta}{\partial M_Z^2}\delta M_Z^2+\frac{\partial\Delta}{\partial M_A^2}\delta M_A^2-\delta M_H^2+\delta M_h^2\right)_\infty \tag{55}$$

where the subscript ∞ on a quantity indicates the "infinite" part of that quantity. Equation (55) implies

$$\delta\beta=(2M_A^2M_Z^2\sin(4\beta))^{-1}\times \tag{56}$$
$$\left((M_Z^2\,\delta M_A^2+M_A^2\,\delta M_Z^2)\cos^2(2\beta)-M_H^2\,\delta M_h^2-M_h^2\,\delta M_H^2\right)_\infty .$$

With this $\overline{MS}$ definition of $\delta\beta$ we introduce a scale dependence into the *CP*-even Higgs-boson masses and the decay rate. However, we have checked that the final results depend insignificantly on this scale; we have chosen the scale $\mu^2=M_Z^2$. This definition of β at one loop gives renormalized *CP*-even Higgs-boson masses in close agreement with those obtained using the effective potential [11] for values of M_A not too close to M_Z. In order to obtain good crossing behavior for the *CP*-even Higgs-boson masses for values of M_A near M_Z a procedure like that of Ref. [12] should be used. In this paper we only consider values of M_A such that $M_A^2/M_Z^2>4$, and the values of the *CP*-even Higgs-boson masses in this region agree favorably with other determinations [11, 12].

The shift in $\delta\beta$ induces a shift in α through equation (35)

$$\delta\alpha = \sin(4\alpha)\left(\frac{\delta\beta}{\sin(4\beta)} + \frac{M_A^2\,\delta M_Z^2 - M_Z^2\,\delta M_A^2}{2(M_A^4 - M_Z^4)}\right). \tag{57}$$

We now come to the renormalization of the HZZ coupling. The bare HZZ and hZZ couplings are given by

$$\lambda_0^{HZZ} = \frac{e_0 M_{Z_0}^3}{M_{W_0}(M_{Z_0}^2 - M_{W_0}^2)^{\frac{1}{2}}}\cos(\beta_0 - \alpha_0), \qquad \lambda_0^{hZZ} = \lambda_0^{HZZ}\tan(\beta_0 - \alpha_0).$$

Defining

$$e_0 = e + \delta e, \qquad Z_{HH}^{\frac{1}{2}} = 1 + \delta Z_{HH}^{\frac{1}{2}}, \qquad (Z_{ZZ}^{\frac{1}{2}})^2 = 1 + \delta Z_{ZZ}$$

(here $Z_{\mu_0} = Z_{ZZ}^{\frac{1}{2}} Z_\mu + Z_{ZA}^{\frac{1}{2}} A_\mu$ where $Z_{\mu_0}(Z_\mu)$ is the bare (renormalized) Z boson field and A_μ is the renormalized photon field) we obtain for the renormalized one loop 3-point function

$$\Gamma_{\mu\nu}^{HZZ} = (\lambda_r^{HZZ} + \lambda_{CT}^{HZZ})g_{\mu\nu} + \Delta\Gamma_{\mu\nu}^{HZZ} \tag{58}$$

where, defining $c_W = M_W/M_Z$, $\lambda_r^{HZZ} = (gM_Z/c_W)\cos(\beta - \alpha_r)$ and

$$\begin{aligned}\lambda_{CT}^{HZZ} = \lambda_r^{HZZ}\Big(&\tfrac{\delta e}{e} + \tfrac{3}{2}\tfrac{\delta M_Z^2}{M_Z^2} - \tfrac{1}{2}\tfrac{\delta M_Z^2 - \delta M_W^2}{M_Z^2 - M_W^2} - \tfrac{1}{2}\tfrac{\delta M_W^2}{M_W^2} \\ &- \tan(\beta - \alpha_r)(\delta\beta - \delta\alpha) + \delta Z_{HH}^{\frac{1}{2}} + \delta Z_{ZZ} + Z_{hH}^{\frac{1}{2}}\tan(\beta - \alpha_r)\Big)\end{aligned} \tag{59}$$

and $\Delta\Gamma_{\mu\nu}^{HZZ}$ is the explicit one loop Feynman diagram contribution (fig. 6). The angle α_r is defined as in Eq. (35), but with the right hand side written in terms of renormalized quantities. The expressions for δM_Z^2, $\delta\beta$, $\delta\alpha$, $Z_{HH}^{\frac{1}{2}}$ and $Z_{hH}^{\frac{1}{2}}$ in terms of self energies and tadpole contributions are given in Eqs. (52), (56), (57) and (47,48). We simply state the results for the remaining shifts δe, δM_W^2 and δZ_{ZZ}. We have

$$\tfrac{\delta e}{e} = \tfrac{1}{2}\Pi_{\gamma\gamma}^{T\,\prime}(0) + \left(\tfrac{4c_W^2 - 3}{4s_W c_W}\right)\tfrac{\Pi_{Z\gamma}^T(0)}{M_Z^2}, \tag{60}$$

$$\delta M_W^2 = \mathrm{Re}\,\Pi_{WW}^T(M_W^2), \qquad \delta Z_{ZZ} = -\mathrm{Re}\,\Pi_{ZZ}^{T\,\prime}(M_Z^2)$$

where $s_W = \sqrt{1-c_W^2}$. We note that $\Pi^T_{Z\gamma}(0)$ vanishes in our case. The H-h mixing gives a contribution to $\Gamma^{\mu\nu}_{HZZ}$ through the term proportional to $Z^{\frac{1}{2}}_{hH}$. The quantity on the right hand side of Eq. (58) is given as a sum of terms which are individually divergent. In the full sum the divergences must of course cancel. We checked both analytically and numerically that this is indeed the case. The renormalizability of the theory requires that the definition of $\delta\beta$ which renders the CP-even Higgs-boson masses finite also gives finite couplings.

The explicit one loop Feynman diagrams shown in fig. 6 give a contribution to the three-point function which can be expanded in terms of form factors as

$$\Delta\Gamma^{\mu\nu}_{HZZ} = D_0 g^{\mu\nu} + D_1 p_1^\mu p_1^\nu + D_2 p_2^\mu p_2^\nu + D_3 p_1^\mu p_2^\nu + D_4 p_2^\mu p_1^\nu \tag{61}$$

(a form factor proportional to $\epsilon^{\mu\nu\alpha\beta} p_{1\alpha} p_{2\beta}$ vanishes by CP invariance). The formula for the decay rate at one loop is

$$\begin{aligned}\Gamma = \sqrt{1-4r}(128\pi r^2 M_H)^{-1} \times \\ \Big\{(1-4r+12r^2)\Big((\lambda_r^{HZZ})^2 \; + \; 2\lambda_r^{HZZ}\mathrm{Re}(\lambda_{CT}^{HZZ}+D_0) + |\lambda_{CT}^{HZZ} \; + \; D_0|^2\Big) \\ + \; M_H^2(1-2r)(1-4r)\Big(\lambda_r^{HZZ}\,\mathrm{Re}(D_4) + \mathrm{Re}[(\lambda_{CT}^{HZZ}+D_0)D_4^*]\Big) \\ + \; M_H^4\left(\frac{1}{2}-2r\right)^2 |D_4|^2\Big\}\end{aligned} \tag{62}$$

where $r = M_Z^2/M_H^2$ and we list D_0 and D_4 in the Appendix.

We note that the terms in the above expression which do not involve λ_r^{HZZ} are formally of $\mathcal{O}(g^6)$. Nevertheless we find that for large Higgs-boson mass ($M_H \gg M_Z$) they are numerically important. This is because λ_r^{HZZ} is proportional to $\cos(\alpha-\beta)$ which is proportional to $1/M_H^2$ for large M_H and hence small. Keeping these $\mathcal{O}(g^6)$ terms is consistent: the terms in the amplitude that are of $\mathcal{O}(g^5)$ which arise at

two loop level also give a contribution of $\mathcal{O}(g^6)$ in the decay rate, but these two loop $\mathcal{O}(g^6)$ terms are proportional to $\cos(\alpha - \beta)$ and are thus suppressed when $M_H \gg M_Z$, in precisely the region where the $\mathcal{O}(g^6)$ terms in our one loop expression become large.

3.3 Discussion

In the MSSM at tree level the decay rate $\Gamma(H \to ZZ)$ is suppressed relative to the same decay rate in the standard model by the factor $\cos^2(\alpha - \beta)$. The "gold-plated" decay mode $H \to ZZ \to 4\ell$ has great discovery potential for a standard model Higgs-boson at a proton super collider such as the SSC for Higgs-boson masses 130 GeV $\lesssim$ M_ϕ $\lesssim$ 800 GeV [16]. The discovery potential for the heavy Higgs-boson of the MSSM in this mode is not as promising due to the above mentioned suppression factor. However, the "gold-plated" mode may be the only discovery mode for the heavy Higgs-boson at a hadron collider [17]. The discovery potential is improved when radiative corrections are taken into account.

We discuss our numerical results below. We have checked our numerics in a number of ways. First, we checked the cancellation of divergences as mentioned in the last section. Second, we found our result for the correction to the neutral Higgs-boson mass sum rule agreed very closely with that of Ref.[7]. Lastly, we checked that our calculation, when modified to give the correction to the standard model Higgs-boson decay rate to two Z's due to an extra heavy fermion doublet, agrees with the results of Ref.[20].

In fig. 7(a) we show the tree level and radiatively corrected decay rate versus the heavy Higgs mass for $\tan\beta$=5 and a top-quark mass of 160 GeV. In this figure we

have not included mixing effects, *i.e.* $A_t = A_b = \mu = 0$ and the squark masses are all equal. We show the corrected rate for the two squark mass choices $M_{sq} = 300$ GeV and $M_{sq} = 1000$ GeV. We see in fig. 7(a) the importance of keeping corrections which are of $\mathcal{O}(g^6)$ in the rate. The one loop corrections which contribute $\mathcal{O}(g^4)$ to the rate fall with M_H (as they multiply the tree level coupling). However, the one loop corrections which contribute $\mathcal{O}(g^6)$ to the rate increase as M_H increases. Hence, these terms eventually dominate the rate as M_H becomes large. In fig. 7(a) the corrected rate is dominated by the $\mathcal{O}(g^4)$ terms for small M_H, and hence it initially falls as M_H increases beyond the kinematic suppression. Eventually, however, the terms of order $\mathcal{O}(g^6)$ become larger than the $\mathcal{O}(g^4)$ terms and the rate then rises with M_H. For $\tan\beta$=5 this begins to occur for values of M_H of about 500 GeV. For larger (smaller) values of $\tan\beta$ the rate begins rising at larger (smaller) values of M_H.

In fig. 7(b) we show the rate versus $\tan\beta$ for a Higgs boson mass of 300 GeV, a top-quark mass of 160 GeV, a squark mass of 1 TeV, and again for no mixing. We see that the corrected rate is approximately twice as large as the tree level value, almost independent of $\tan\beta$. As we will discuss below, the rate depends dramatically on $\tan\beta$ once mixing is included.

In fig. 8 the ratio of the radiatively corrected rate to the tree level rate is shown versus the top-quark mass, for the same set of parameters as fig. 7(b), and $\tan\beta$=5. Fig. 8 illustrates that the corrected rate depends strongly on two parameters in the case of no mixing. Clearly the rate depends on the value of the top-quark mass. But note for M_H=1 TeV that even for a top-quark mass as small as 100 GeV the corrected rate is still over a factor of two larger than at tree level. Thus the relative

size of the correction depends greatly on the value of M_H as well. Note, however, that when the top-quark mass is less than around 120 GeV we expect that the corrections from other sectors will be of the same order of magnitude as the correction due to the quark/squark sector included here.

When mixing is included the parameter space increases. We will choose a point in mixing space and examine the effect of mixing in deviations from that point. We choose $A-$terms $A_t = A_b = 600$ GeV and squark masses $\tilde{m}_{t_1} = \tilde{m}_{b_1} = 600$ GeV, and $\tilde{m}_{t_2} = \tilde{m}_{b_2} = 300$ GeV. Additionally, we will consider the two cases $\mu = \pm 400$ GeV. In all three of the figures 9, 10, and 11 the heavy Higgs-boson mass is set to 300 GeV and the top quark mass is 160 GeV. In order to isolate the effect of mixing we will plot the ratio of the corrected rate including mixing to the corrected rate with no mixing (where the common squark mass is set to 600 GeV). In figs. 9 we plot this ratio vs. the squark mass $\tilde{m}_{t_1}$. We find that the effect due to mixing is strongly dependent on $\tan\beta$ and μ. For large values of $\tan\beta$ the effects of mixing are greatly enhanced. As shown in figs. 9, the inclusion of mixing can change the rate by a factor 1.3 for $\tan\beta$=2 and for $\tan\beta$=20 by a factor 2.7 or 0.3, for $\mu = -400$ GeV or $\mu = +400$ GeV, respectively.

Similar ratios are seen in figs. 10, where the ratio of the corrected rate including mixing to the corrected rate with no mixing is shown vs. A_t, the top squark mixing parameter. As in figs. 9 the two curves for $\mu = \pm 400$ GeV are similar when $\tan\beta$=2; the rate can be increased by 50% or decreased by 25%. If $\tan\beta$=20 the effects of mixing are more pronounced and the ratio varies between roughly 1/3 and 3. The curves in fig. 10(a) (and fig. 11(a)) do not span the entire ordinate axis shown because unphysical regions of the squark mixing parameter space are encountered.

In fig. 11 we plot the (mixing) to (no mixing) ratio vs. the supersymmetric Higgs mass parameter μ. We see there is little dependence on μ for small $\tan\beta$, while for larger values of $\tan\beta$ the dependence is quite significant. If $\tan\beta$=20 the ratio varies between 4 and 1/36 as μ varies from -750 to 750 GeV. Finally, we note that there is very little dependence on the bottom squark masses and $A-$term A_b for the mixing configurations considered.

To summarize, we have computed the one loop corrections to the decay rate $\Gamma(H \to ZZ)$ in the MSSM including third family quark and squark loops. We perform a Feynman diagram calculation in the on-mass-shell renormalization scheme. As the tree level rate falls like $1/M_H$ for large M_H and we find corrections that grow with M_H, the corrected rate may be many times the tree level rate. For example, at $M_H = 1$ TeV the corrected rate may be 13 times the uncorrected rate for m_t=200 GeV (with no squark mixing). The corrected rate depends very strongly on the squark mixing parameters. For example, for the mixing configuration considered here, the rate varies by two orders of magnitude as the Higgs mass parameter μ varies between $\pm$750 GeV. Indeed, the squark mixing parameters μ, A_t, and the top squark masses, in addition to the top-quark mass, must be measured in order to test the Higgs sector of the MSSM.

4 The branching ratios of the heavy Higgs-boson

4.1 Introduction

In this section we consider radiative corrections to all the relevant two–body decay modes of the heavy Higgs-boson, assuming that all the supersymmetric de-

cay modes are kinematically inaccessible. Thus we consider the fermionic decays $H \to t\bar{t}$, $b\bar{b}$, $\tau^+\tau^-$, $c\bar{c}$, the decays to vector boson pairs $H \to W^+W^-$, ZZ, gg, $\gamma\gamma$ and decays to Higgs-bosons $H \to hh$, AA. In this chapter we will set the top mass to m_t =150 GeV. There is a window at small values of M_A where the decay $H \to AZ$ occurs but we do not include this decay mode in our analysis.

Of course the decay rates to gg and $\gamma\gamma$ are zero at tree level. The formulas for these rates at the one–loop level can be found in Ref. [16]. In determining the $\gamma\gamma$ rate we include the contributions from three generations of quarks and charged leptons and their supersymmetric partners, the W boson, the charged Higgs-boson and the charginos. We set the slepton masses equal to 1 TeV. For the chargino case we set the wino mass parameter to $M = 500$ GeV. We will in some cases consider the Higgsino mass parameter μ to be zero (or small), and hence a chargino will be lighter than the present experimental lower bound of 45 GeV [21], but in any case the chargino contribution to the $\gamma\gamma$ rate is not large. For the gg rate we simply include three generations of quarks and squarks. We assume the first and second generations of squarks are degenerate with the third. Naturally the third generation quark and squark contributions are largest.

Including quark and squark corrections to the fermionic decay rates gives generically small ($\mathcal{O}(10\%)$) corrections. There are no explicit three point diagrams in these cases. The corrections arise from wave–function and counter–term renormalization. We expect that the corrections due to other sectors of the theory will be of the same order of magnitude as the corrections we include. In the case of $t\bar{t}$, $b\bar{b}$ and $c\bar{c}$ decays we include QCD corrections [22]. These corrections can be quite large for the bottom and charm quarks due to running mass effects, for example reducing the $b\bar{b}$

rate by ~50%.

The renormalization of the W^+W^- decay rate is very similar to the ZZ rate shown in detail in the previous chapter. The normalization of the renormalized W^+W^- is generically two to three times as large as the ZZ rate and, qualitatively, the two corrected rates have the same shape. In particular, the corrected W^+W^- rate also overcomes the tree–level suppression that occurs at large values of M_H, and dramatically rises for sufficiently large values of M_H.

4.2 General features

We will examine the heavy Higgs branching ratios for two representative values of $\tan\beta$. In this section we will specify, rather than squark masses, the squark mass parameters M_U, M_D, and M_Q. The squark masses are then given by

$$\tilde{m}^2_{t_{1,2}} = m_t^2 + \frac{1}{2}(M_Q^2 + M_U^2) + \frac{1}{4}M_Z^2\cos 2\beta \pm\sqrt{\left(\frac{M_Q^2 - M_U^2}{2} + \frac{8M_W^2 - 5M_Z^2}{12}\cos 2\beta\right)^2 + m_t^2(A_t + \mu\cot\beta)^2} \tag{63}$$

$$\tilde{m}^2_{b_{1,2}} = m_b^2 + \frac{1}{2}(M_Q^2 + M_D^2) - \frac{1}{4}M_Z^2\cos 2\beta \pm\sqrt{\left(\frac{M_Q^2 - M_D^2}{2} - \frac{4M_W^2 - M_Z^2}{12}\cos 2\beta\right)^2 + m_b^2(A_b + \mu\tan\beta)^2}. \tag{64}$$

If we refer to a value of M_{sq} then we have set the quark mass parameters to be equal, *i.e.* $M_{sq} = M_U = M_D = M_Q$. Similarly, if we refer to a value of A, we implicitly refer to both the top and bottom A-terms, and they are equal.

We show in figures 12(a,b) the branching ratios for $\tan\beta = 2$, $M_{sq} = 1$ TeV and $A = \mu = 0$. In this figure it is shown that the decay $H \to AA$ is only accessible near the endpoint of the M_H parameter space. However, whenever this decay mode

is allowed the rate is substantial. The decay to hh is also quite substantial, and it is the dominant decay rate for values of M_H below the $t\bar{t}$ threshold, except in a small region near $M_H = 132$ GeV where the (renormalized) Hhh coupling vanishes. (At tree level this zero occurs at $M_H = 104$ GeV.) The branching ratio of the phenomenologically interesting decay mode $H \to ZZ$ is roughly 6.8% below the top threshold. Requiring the two Z-bosons to decay to e or μ pairs (the "gold–plated" mode) reduces this branching ratio to the 10^{-4} level. Note that this level of branching ratio is sufficient to detect the heavy Higgs–boson at the SSC or LHC. Of course, the ZZ branching ratio initially drops for values of M_H above the top threshold, making detection in this region difficult or impossible. At very high values of M_H we find that the ZZ branching ratio begins to rise. If $\tan\beta = 2$ this begins to occur near M_H=600 GeV. However, the rate does not rise sufficiently fast to compensate for the decrease suffered when crossing the top threshold. Even at M_H=1200 GeV the ZZ branching ratio is still an order of magnitude less than its value before the top threshold. It should be emphasized that even if the branching ratio were an order of magnitude larger, the orders of magnitude decrease in the production cross section of such heavy Higgs–bosons would make detection impossible.

If we consider smaller squark masses, e.g. $M_{sq} = 300$ GeV, we find qualitatively the same picture. The major differences are that the lower limit for M_H is decreased to about $M_{H_{min}}$=101 GeV, down from $M_{H_{min}}$=116 GeV when $M_{sq} = 1$ TeV; the value of M_H where the Hhh coupling vanishes is correspondingly smaller than the large squark mass case; and the all of the branching ratios except the dominant one (hh below the top threshold) are decreased by about 20%.

In figures 13(a,b) we show branching ratios for the same values of parame-

ters as figure 12, but for $\tan\beta = 20$. At large values of $\tan\beta$ the coupling of the heavy Higgs–boson to down–type fermions is enhanced by the factor $1/\cos\beta$. Consequently, the $b\bar{b}$ branching ratio completely dominates the figure, even above the $t\bar{t}$ threshold, while the $\tau^+\tau^-$ ratio is the second largest at about 7%. Note that the AA decay mode is only allowed near the endpoint $M_H = M_{H_{min}}$. In fact, this curve would appear as a dot on fig. 13, so we do not include it. Similarly, $H \to hh$ is allowed at this endpoint. These two decay modes have the largest rates at the endpoint and each have branching ratios of 49%. At this large value of $\tan\beta$ the ZZ branching ratio (not including the branching ratios for both Z's to decay to e or μ) is only at most at the 10^{-4} level and thus detection via the "gold–plated" mode is impossible at the LHC or SSC. Beyond the top and hh thresholds the ZZ branching ratio begins to rise for values of $M_H \gtrsim 900$ GeV. This rise is far too mild to be of phenomenological interest.

4.3 Squark mixing effects

We determined in the previous chapter that the radiatively corrected decay rate $H \to ZZ$ can vary by two orders of magnitude for various values of the squark mixing parameters. We now determine if such variances appear in the branching ratios as well. We will, as in the previous chapter, pick a point in squark mixing parameter space and show the results for various branching ratios as we vary individual squark mixing parameters away from that point. We will display the results as ratios of the branching ratio for the mixed configuration divided by the branching ratio for a specific unmixed configuration. The unmixed configuration we choose has $A = \mu = 0$ and $M_{sq} = 600$ GeV. The mixed configuration corresponds to $A = 600$ GeV,

$M_Q = 600$ GeV, $M_U = 300$ GeV, $M_D = 900$ GeV, and $\mu = \pm 700$ GeV. We will fix the heavy Higgs–boson mass at $M_H = 260$ GeV for the remainder of this discussion.

In figure 14 we show the results for the ratio of the mixed branching ratios to the unmixed branching ratios vs. the top squark mass parameter M_U. As will be the case for the next two figures, we show the results for $\tan\beta = 2$ and 20 in figs. (a) and (b), respectively. We see that, as was the case for the ZZ decay rate, the branching ratio dependence on the squark mass parameters increases dramatically when $\tan\beta$ gets large. At $\tan\beta = 2$ the branching ratios in the mixed configuration differ by those of the unmixed configuration by $\lesssim$10% for $M_U > 350$ GeV. For lower values of M_U differences of roughly 50% can be seen for the hh and $b\bar{b}$ branching ratios, with the largest differences occurring when M_U reaches the edge of physical squark mass parameter space. At this edge of parameter space the $\gamma\gamma$ branching ratio is $\frac{1}{10}$ of its value in the unmixed configuration. We remark that the results for the $\tau^+\tau^-$ mode are, in this and the next two figures, found to be nearly identical to the results shown for the $b\bar{b}$ mode. Similarly, the W^+W^- and ZZ curves are very similar. For $\tan\beta$ =20 and $\mu = 700$ GeV the ZZ, W^+W^-, and hh modes all vary by two orders of magnitude as M_U varies from 180 to 1000 GeV. In the case $\mu = -700$ GeV the same three branching ratios are a factor 2 to 4 larger than the unmixed branching ratios as M_U varies over the same interval. At such large values of $\tan\beta$ the other branching ratios are only mildly dependent on the the squark mixing parameters.

In figures 15(a,b) we show the ratio of the branching ratios including mixing to the branching ratios without mixing as a function of A_t, for μ=700 GeV. We note that the plots corresponding to the case $\mu = -700$ GeV are very similar to

those shown in figures 15, except that $A_t \to -A_t$. In figure 15(a) we show, for $\tan\beta$ =2, the ratio of branching ratios corresponding to the ZZ, hh, $b\bar{b}$, and $\gamma\gamma$ decay modes. As in the figure 14(a), we find that at such a low value of $\tan\beta$ the dependence is relatively mild ($\lesssim$30%) unless one considers values of A_t very near the edge of the physically allowed parameter space. In this case the endpoint region is near A_t=1000 GeV, and near these values of A_t the branching ratios with mixing included can be reduced by a factor of 10 when compared to the branching ratios evaluated with no squark mixing. Naturally, we do not *expect* the squark mixing parameters to have values very near the edge of the allowed parameter space. In the case $\tan\beta$ =20, shown in figure 15(b), again the branching ratios corresponding to the ZZ, hh, and WW decay modes are quite sensitive to the value of the squark mixing parameters, while the other branching ratios are not. As A_t varies from -700 to 600 GeV the ZZ, W^+W^-, and hh branching ratios are roughly a factor 3 to $\frac{1}{20}$ times the corresponding branching ratios in the unmixed case.

In figures 16(a,b) we show the dependence of the branching ratios on the Higgs mass parameter μ. We see in figure 16(a) that, even at the relatively small value of $\tan\beta$ =2, the $b\bar{b}$ and $\gamma\gamma$ branching ratios can be reduced by two orders magnitude when μ is near its upper limit of $\sim$1400 GeV. However, if we restrict the parameter space to $|\mu| < 600$ GeV, we find that the various branching ratios all differ from the branching ratios in the no–mixing case by $\lesssim$20%. If $\tan\beta$ =20, of course we expect a larger dependence. This is demonstrated in figure 16(b), where the hh, ZZ, and W^+W^- branching ratios are seen to encounter severe dips near the region μ = 900 GeV. At extremely large and negative values of μ ($\mu \sim -2$ TeV) these three branching ratios are 8 or 9 times larger than in the unmixed case.

To conclude, we find large variations in the branching ratios of the heavy Higgs-boson when varying the squark mixing parameters. For $\tan\beta = 2$ the ratio of the branching ratios including squark mixing effects to the branching ratios with no squark mixing are generally small ($\sim 20\%$) unless a squark mixing parameter approaches the edge of the physically allowed parameter space. At larger values of $\tan\beta$ the dependence on squark mixing can be quite large for the ZZ, W^+W^- and hh decay modes. The branching ratios corresponding to these modes can be suppressed by orders of magnitude (or enhanced by a factor 10) when squark mixing is considered. Thus, the squark mixing parameters must be measured in order to make precise predictions concerning the properties of the heavy Higgs-boson in the minimal supersymmetric model.

Appendix

In this Appendix we give explicit analytic expressions for the self energies, tadpoles, and form factors introduced in the text. Our expressions are given in terms of the standard A, B, C functions introduced by Passarino and Veltman [18] which appear in one loop calculations. We adopt the metric $(1, -1, -1, -1)$, which is different than that of Ref.[18]. Explicit analytic formulas for these functions appear in Ref.[19].

To make the equations more concise we adopt the following conventions. N_c denotes the number of quark colors. The index α runs over the top and bottom sectors while the indices i, j, and k run over squark mass eigenstates. Thus, m_α denotes a quark mass while $\tilde{m}_{\alpha i}$ denotes a squark mass. For the A and B functions we define $A_\alpha = A(m_\alpha^2)$, $\tilde{A}_{\alpha i} = A(\tilde{m}_{\alpha i}^2)$, $B_{0_\alpha} = B_0(p^2, m_\alpha^2, m_\alpha^2)$, $\tilde{B}_{0_{\alpha ij}} = B_0(p^2, \tilde{m}_{\alpha i}^2, \tilde{m}_{\alpha j}^2)$ and similarly for the rest of the B's. A C function has six arguments: three external squared momenta and the three squared masses of the particles which appear in loop of the 3-point diagram. We thus define $\tilde{C}_{0_{\alpha ijk}} = C_0(M_Z^2, M_Z^2, M_H^2, \tilde{m}_{\alpha i}^2, \tilde{m}_{\alpha j}^2, \tilde{m}_{\alpha k}^2)$ and $C_{0_\alpha} = C_0(M_Z^2, M_Z^2, M_H^2, m_\alpha^2, m_\alpha^2, m_\alpha^2)$ with analogous definitions for the rest of the C's.

First we give expressions for the Higgs-boson self energies.

$$\Pi_{HH}(p^2) = N_c \textstyle\sum_{\alpha ij} (\tilde{V}_{\alpha ij}^H)^2 \tilde{B}_{0_{\alpha ij}} - N_c \textstyle\sum_{\alpha i} \tilde{U}_{\alpha ii}^{HH} \tilde{A}_{\alpha i} \tag{65}$$

$$-12 N_c \textstyle\sum_\alpha (V_\alpha^H)^2 \Big(m_\alpha^2 B_{0_\alpha} + p^2 (B_{21_\alpha} - B_{1_\alpha}) + \tfrac{1}{48\pi^2} (m_\alpha^2 - \tfrac{p^2}{6}) \Big).$$

The various V and U vertex factors are shown in fig. 18 and explicit expressions appear in Refs.[1, 16]. However, the H-h-$\tilde{q}_{kL}$-$\tilde{q}_{kL}$ and H-h-$\tilde{q}_{kR}$-$\tilde{q}_{kR}$ vertices given in

Ref.[16] are incorrect. In the notation of Ref.[16] the above couplings are

$$\frac{ig^2\sin 2\alpha}{4}\left(2\frac{T_{3k}-e_k\sin^2\theta_W}{\cos^2\theta_W}-\frac{m_q^2}{M_W^2}D_k\right) \quad \text{and} \quad \frac{ig^2\sin 2\alpha}{4}\left(2e_k\tan^2\theta_W-\frac{m_q^2}{M_W^2}D_k\right)$$

respectively ($D_{up}=1/\sin^2\beta$, $D_{down}=-1/\cos^2\beta$).

Π_{hh} is given as Π_{HH} with $\tilde{V}^H_{\alpha ij}\to\tilde{V}^h_{\alpha ij}$, $\tilde{U}^{HH}_{\alpha ii}\to\tilde{U}^{hh}_{\alpha ii}$, and $V^H_\alpha\to V^h_\alpha$. Π_{Hh} is given as Π_{HH} with $(\tilde{V}^H_{\alpha ij})^2\to\tilde{V}^h_{\alpha ij}\tilde{V}^H_{\alpha ij}$, $\tilde{U}^{HH}_{\alpha ii}\to\tilde{U}^{Hh}_{\alpha ii}$, and $(V^H_\alpha)^2\to V^H_\alpha V^h_\alpha$. Π_{AA} is given as Π_{HH} with $\tilde{V}^H_{\alpha ij}\to\tilde{V}^A_{\alpha ij}$, $\tilde{U}^{HH}_{\alpha ii}\to\tilde{U}^{AA}_{\alpha ii}$, $V^H_\alpha\to V^A_\alpha$, and $B_{0_\alpha}\to\frac{1}{3}B_{0_\alpha}$. Next we list the transverse part of the gauge boson self energies.

$$\begin{aligned}\Pi^T_{ZZ}(p^2) &= N_c\sum_{\alpha i}\tilde{U}^{ZZ}_{\alpha ii}\tilde{A}_{\alpha i} \\ &- 2N_c\sum_{\alpha ij}(\tilde{V}^Z_{\alpha ij})^2\Big(\tilde{m}^2_{\alpha i}\tilde{B}_{0_{\alpha ij}}-(\tilde{m}^2_{\alpha i}-\tilde{m}^2_{\alpha j}+p^2)\tilde{B}_{1_{\alpha ij}} \\ &\qquad + p^2\tilde{B}_{21_{\alpha ij}}+\frac{1}{16\pi^2}\Big(\frac{\tilde{m}^2_{\alpha i}+\tilde{m}^2_{\alpha j}}{2}-\frac{p^2}{6}\Big)\Big) \\ &- 8N_c\sum_\alpha\Big((V^Z_{5\alpha})^2m^2_\alpha B_{0_\alpha}+\big((V^Z_\alpha)^2+(V^Z_{5\alpha})^2\big)p^2(B_{21_\alpha}-B_{1_\alpha})\Big)\end{aligned} \tag{66}$$

$$\begin{aligned}\Pi^T_{WW}(p^2) &= N_c\sum_{\alpha i}\tilde{U}^{WW}_{\alpha ii}\tilde{A}_{\alpha i} \\ &- 2N_c\sum_{ij}(\tilde{V}^W_{ij})^2\Big(\tilde{m}^2_{ti}\tilde{B}^W_{0_{ij}}-(\tilde{m}^2_{ti}-\tilde{m}^2_{bj}+p^2)\tilde{B}^W_{1_{ij}} \\ &\qquad + p^2\tilde{B}^W_{21_{ij}}+\frac{1}{16\pi^2}\Big(\frac{\tilde{m}^2_{ti}+\tilde{m}^2_{bj}}{2}-\frac{p^2}{6}\Big)\Big) \\ &- 8N_c(V^W)^2\Big(m^2_tB^W_0-(m^2_t-m^2_b+2p^2)B^W_1+2p^2B^W_{21}\Big)\end{aligned} \tag{67}$$

where $\tilde{B}^W_{ij}=B(p^2,\tilde{m}^2_{t_i},\tilde{m}^2_{b_j})$ and $B^W=B(p^2,m^2_t,m^2_b)$. $\Pi^T_{\gamma\gamma}$ is given as Π^T_{ZZ} with $\tilde{V}^Z_{\alpha ij}\to\tilde{V}^\gamma_{\alpha ij}$, $\tilde{U}^{ZZ}_{\alpha ii}\to\tilde{U}^{\gamma\gamma}_{\alpha ii}$, $V^Z_\alpha\to V^\gamma_\alpha$, $V^Z_{5\alpha}\to 0$. The heavy Higgs-boson tadpole contribution is given by

$$T_H=N_c\Big(4\sum_\alpha V^H_\alpha m_\alpha A_\alpha-\sum_{\alpha i}\tilde{V}^H_{\alpha ii}\tilde{A}_{\alpha i}\Big). \tag{68}$$

T_h is given as T_H with $\tilde{V}^H_{\alpha ii} \to \tilde{V}^h_{\alpha ii}$ and $V^H_\alpha \to V^h_\alpha$. Lastly, the two three-point Feynman diagram form factors which are relevant for calculating the Higgs-boson decay rate are

$$
\begin{aligned}
D_0 = {} & 8N_c \sum_\alpha m_\alpha V^H_\alpha ((V^Z_\alpha)^2 + (V^Z_{5\alpha})^2) \\
& \times \Big(4C_{24_\alpha} + (M_H^2 - 2M_Z^2) C_{12_\alpha} + 2M_Z^2 C_{11_\alpha} - \frac{M_H^2}{2} C_{0_\alpha} - B_0(M_Z^2, m_\alpha^2, m_\alpha^2) \Big) \\
& + \; 8N_c \sum_\alpha m_\alpha V^H_\alpha (V^Z_{5\alpha})^2 \Big(\left(M_H^2 - 4m_\alpha^2 \right) C_{0_\alpha} - 2B_0(M_Z^2, m_\alpha^2, m_\alpha^2) \Big) \qquad (69) \\
& - \; 8N_c \sum_{\alpha ijk} \tilde{V}^H_{\alpha ki} \tilde{V}^Z_{\alpha ij} \tilde{V}^Z_{\alpha jk} \tilde{C}_{24_{\alpha ijk}} \; + \; N_c \sum_{\alpha ij} \tilde{V}^H_{\alpha ij} \tilde{U}^{ZZ}_{\alpha ij} B_0(M_H^2, \tilde{m}^2_{\alpha i}, \tilde{m}^2_{\alpha j})
\end{aligned}
$$

and

$$
\begin{aligned}
D_4 = {} & 8N_c \sum_\alpha m_\alpha V^H_\alpha \Big(\left((V^Z_\alpha)^2 + (V^Z_{5\alpha})^2 \right) (4C_{23_\alpha} + C_{0_\alpha} - 4C_{12_\alpha}) - 2(V^Z_{5\alpha})^2 \left(C_{11_\alpha} - C_{12_\alpha} \right) \Big) \\
& - \; 8N_c \sum_{\alpha ijk} \tilde{V}^H_{\alpha ki} \tilde{V}^Z_{\alpha ij} \tilde{V}^Z_{\alpha jk} \left(\tilde{C}_{23_{\alpha ijk}} - \tilde{C}_{12_{\alpha ijk}} \right). \qquad (70)
\end{aligned}
$$

References

[1] H.E. Haber and G.L. Kane, *Phys. Rep.* **117** (1985) 75.

[2] H.P. Nilles, *Phys. Rep.* **110** (1984) 1;

J.F. Gunion and H.E. Haber, *Nucl. Phys.* **B272** (1986) 1.

[3] S.P. Li and M. Sher, *Phys. Lett.* **B140** (1984) 339;

Y. Okada, M.Yamaguchi and T. Yanagida, *Prog. Theor. Phys. Lett.* **85** (1991) 1; *Phys. Lett.* **B262** (1991) 54;

J. Ellis, G. Ridolfi and F. Zwirner, *Phys. Lett.* **B257** (1991) 83;

H.E. Haber and R. Hempfling, *Phys. Rev. Lett.* **66** (1991) 1815;

R. Barbieri, M. Frigeni and M. Caravaglios, *Phys Lett.* **B258** (1991) 167;

R. Barbieri, M. Frigeni, *Phys Lett.* **B258** (1991) 395;

A. Yamada, *Phys. Lett.* **B263** (1991) 233;

P.H. Chankowski, preprint IFT-7-91-WARSAW, Institute of Theoretical Physics, Warsaw University 00-681, Hoza 69, Warsaw, Poland, 1991 (unpublished);

J.R. Espinosa and M. Quirós, *Phys. Lett.* **B266** (1991) 389;

J.L. Lopez and D.V. Nanopoulos, *Phys. Lett.* **B266** (1991) 397;

Z. Kunszt and F. Zwirner, to appear in Proc. of Large Hadron Collider Workshop, Aachen, Germany, Oct. 4-9, 1990.

[4] J. Ellis, G. Ridolfi and F. Zwirner, *Phys. Lett.* **B262** (1991) 477.

[5] A. Brignole, J. Ellis, G. Ridolfi and F. Zwirner, *Phys. Lett.* **B271** (1991) 123.

[6] J.F. Gunion and A. Turski, *Phys. Rev.* **D39** (1989) 2701; **D40** (1990) 2333.

[7] M.S. Berger, *Phys. Rev.* **D41** (1990) 225.

[8] S. Coleman and E. Weinberg, *Phys. Rev.* **D7** (1973) 1883.

[9] M.K. Gaillard, *Nucl. Phys.* **B268** (1986) 669;

J.W. Burton, V. Jain, and M.K. Gaillard, *Phys. Rev.* **D41** (1990) 3118.

[10] D. Decamp *et al.*, ALEPH Coll., preprint CERN-PPE/91-111, Organisation Européenne Pour La Recherche Nucléaire, 1991 (to be published).

[11] D.M. Pierce, A. Papadopoulos and S.B. Johnson, *Phys. Rev. Lett.* **25** (1992) 3678.

[12] A. Brignole, *Phys. Rev. Lett.* **B281**, (1992) 284.

[13] V.Barger, M.S. Berger, A.L. Stange and R.J.N. Phillips, *Phys. Rev.* **D45**, (1992) 4128.

[14] J.F. Gunion, R. Bork, H.E. Haber and A. Seiden, *Phys. Rev.* **D46**, (1992) 2040.

[15] K. Aoki, Z. Hioki, R. Kawabe, M. Konuma and T. Muta, *Prog. Theor. Phys.***73**, Suppl. (1982) 1.

[16] J.F. Gunion, H.E. Haber G. Kane and S. Dawson, *The Higgs Hunter's Guide,* Addison-Wesley Publishing Company, Redwood City, CA, 1990.

[17] J.F. Gunion, preprint UCD-91-22 (1991), to appear in Proc. of QCD at 200-TeV conf., Erice, Italy, June 11-17, 1991.

[18] G. Passarino and M. Veltman, *Nucl. Phys.* **B160** (1979) 151.

[19] G. 't Hooft and M. Veltman, *Nucl. Phys.* **B153** (1979) 365; see also Ref.[20].

[20] B.A. Kniehl, *Nucl. Phys.* **B352** (1991) 1.

[21] K. Hidaka, *Phys. Rev.* **D44** (1991) 927.

[22] S.G. Gorishny *et al.*, *Mod. Phys. Lett.* **A5** (1990) 2703.

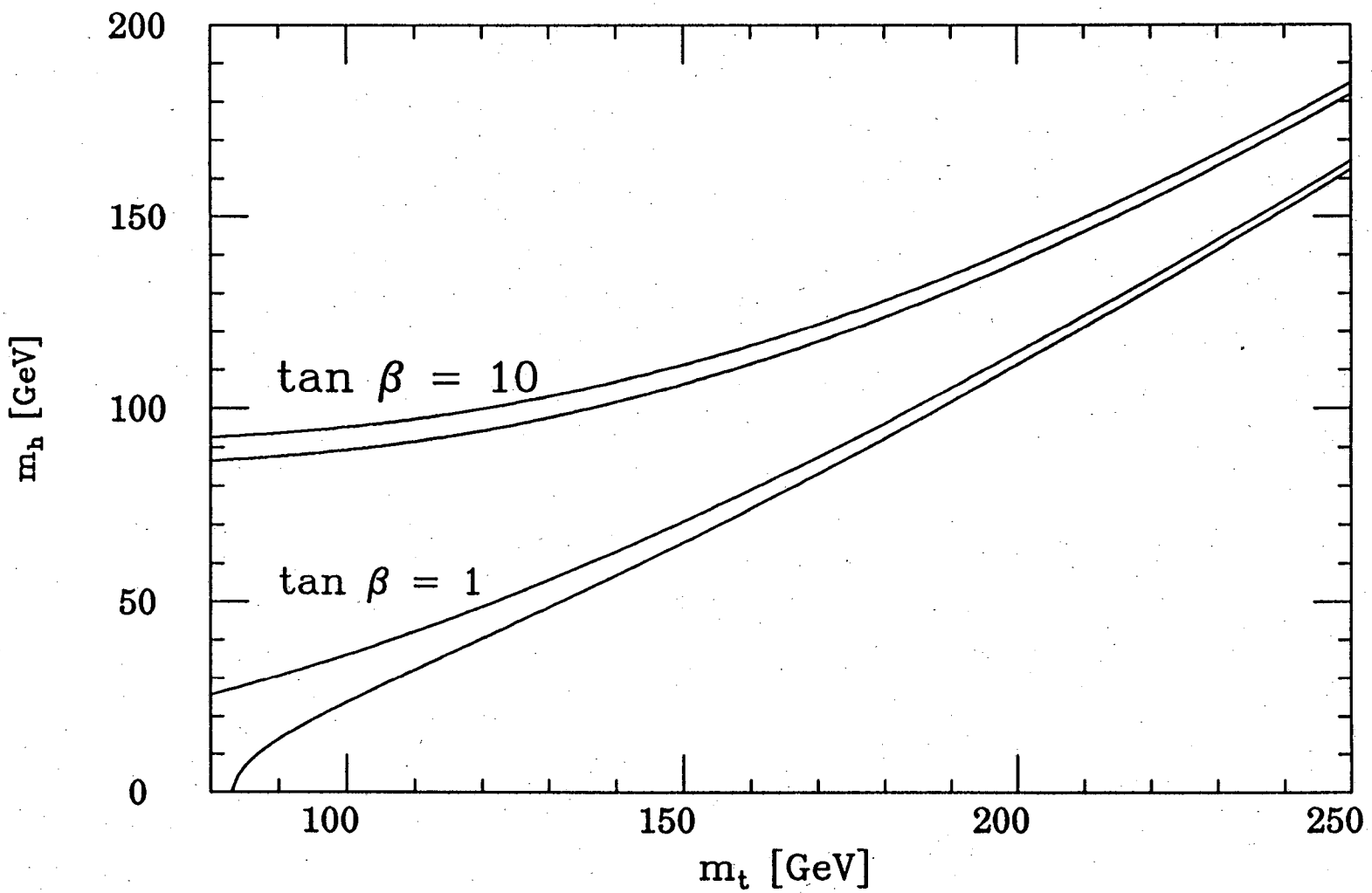
200
150
100
50
0
100
150
200
250
m_h [GeV]
m_t [GeV]
tan β = 10
tan β = 1

Figure 1(a)

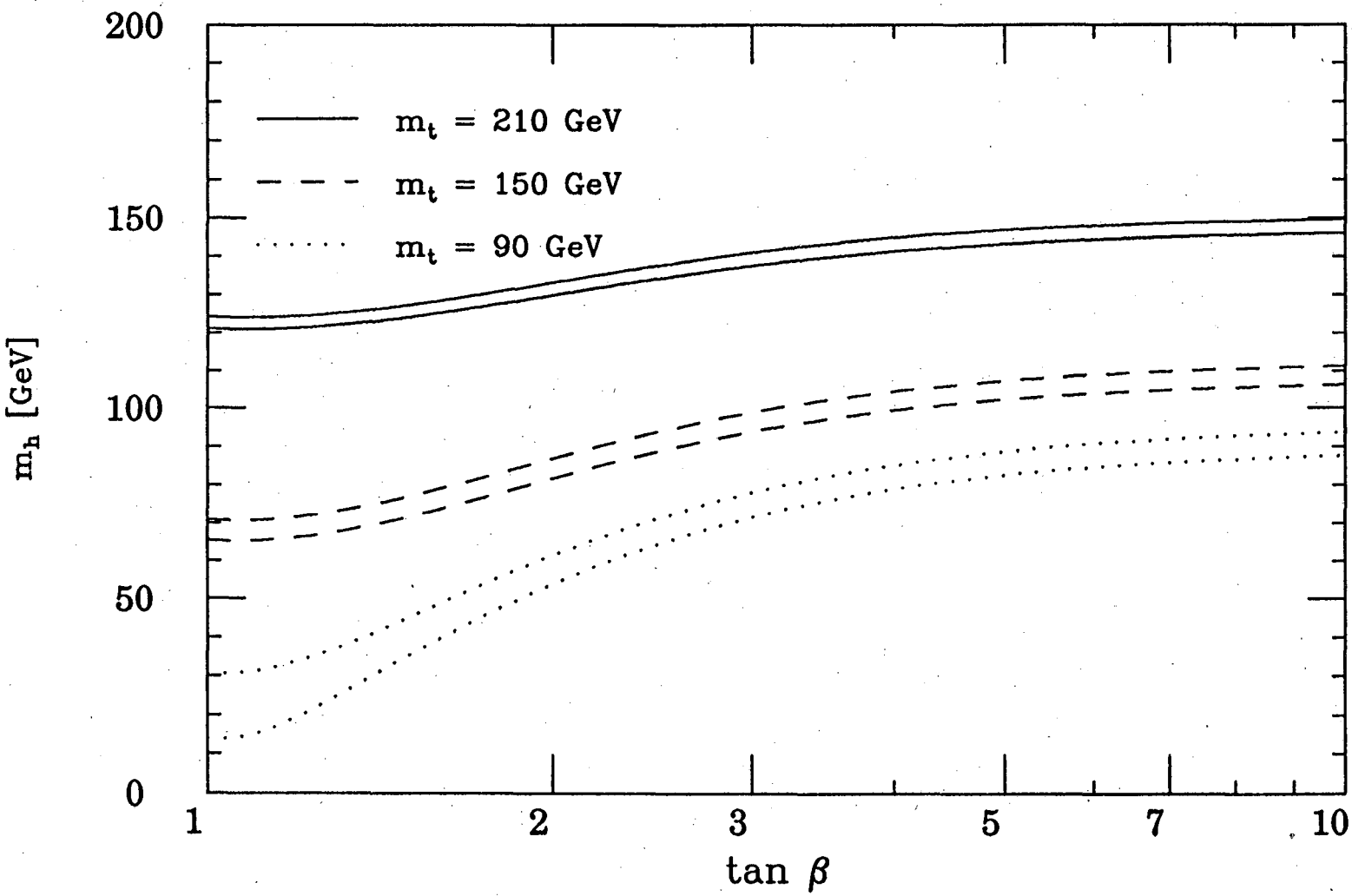
200
150
100
50
0
m_h [GeV]
1
2
3
5
7
10
tan β
m_t = 210 GeV
m_t = 150 GeV
m_t = 90 GeV

Figure 1(b)

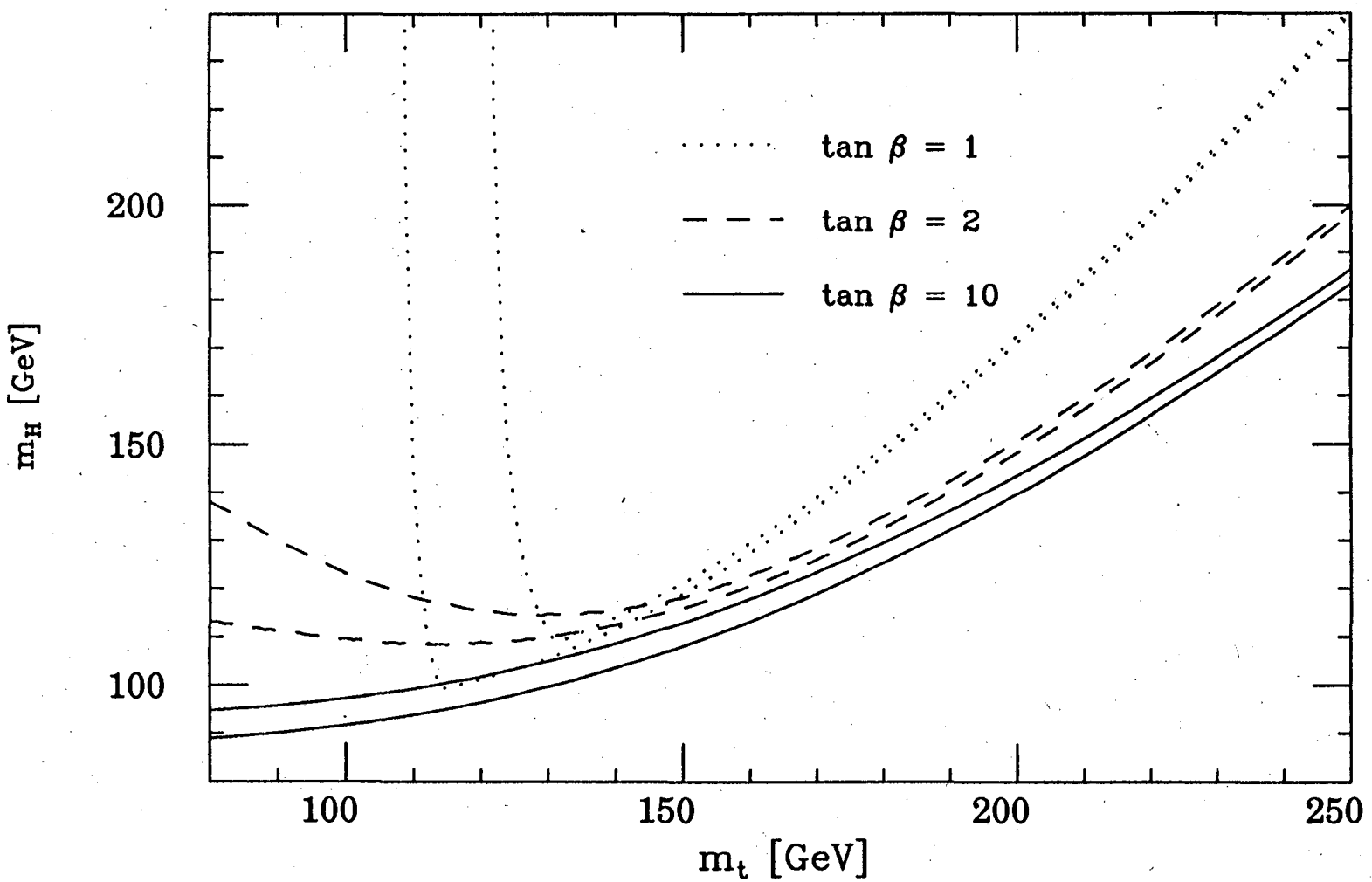

Figure 2(a)

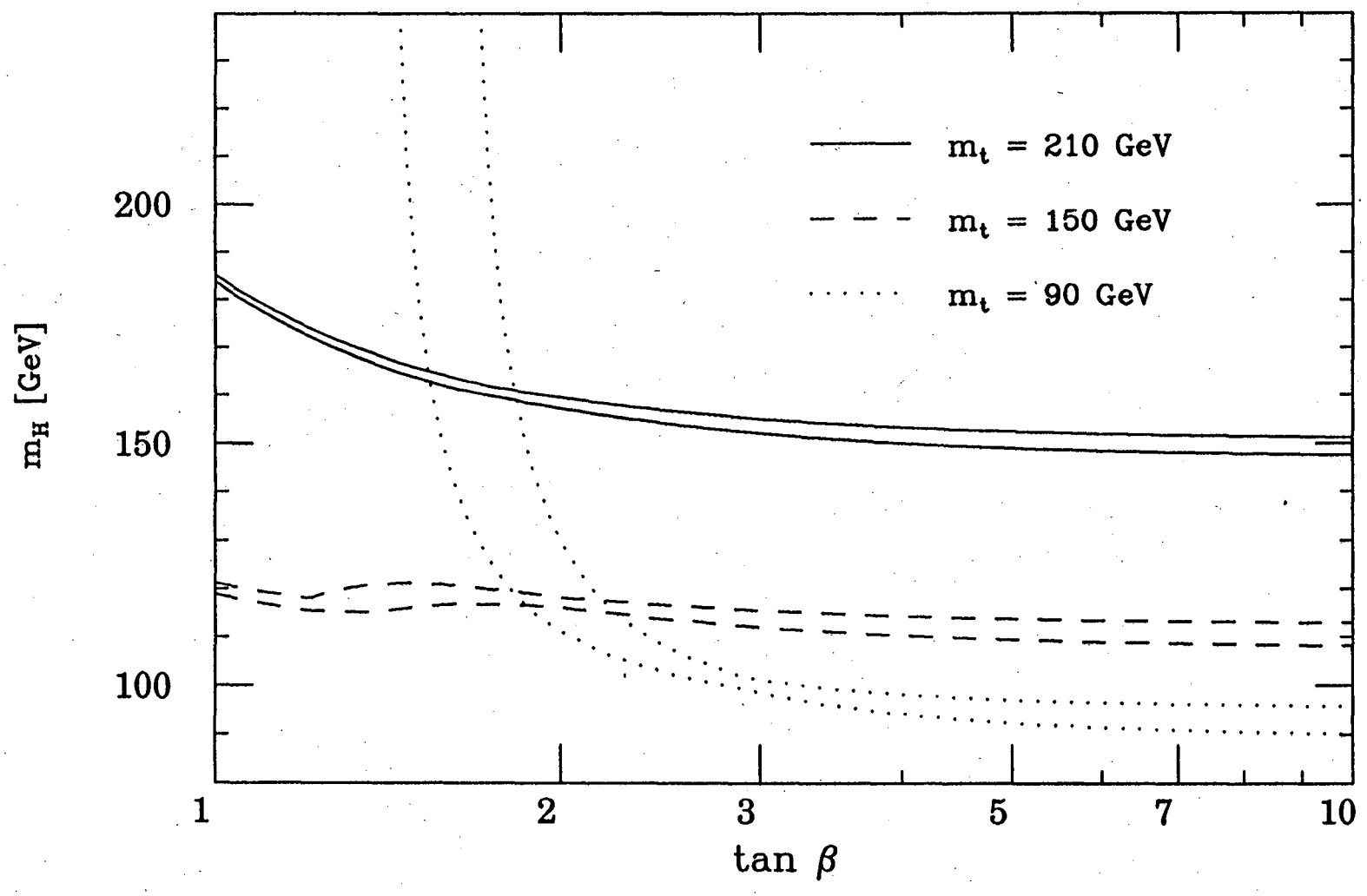
m_t = 210 GeV
m_t = 150 GeV
m_t = 90 GeV
200
150
100
m_H [GeV]
1
2
3
5
7
10
tan β

Figure 2(b)

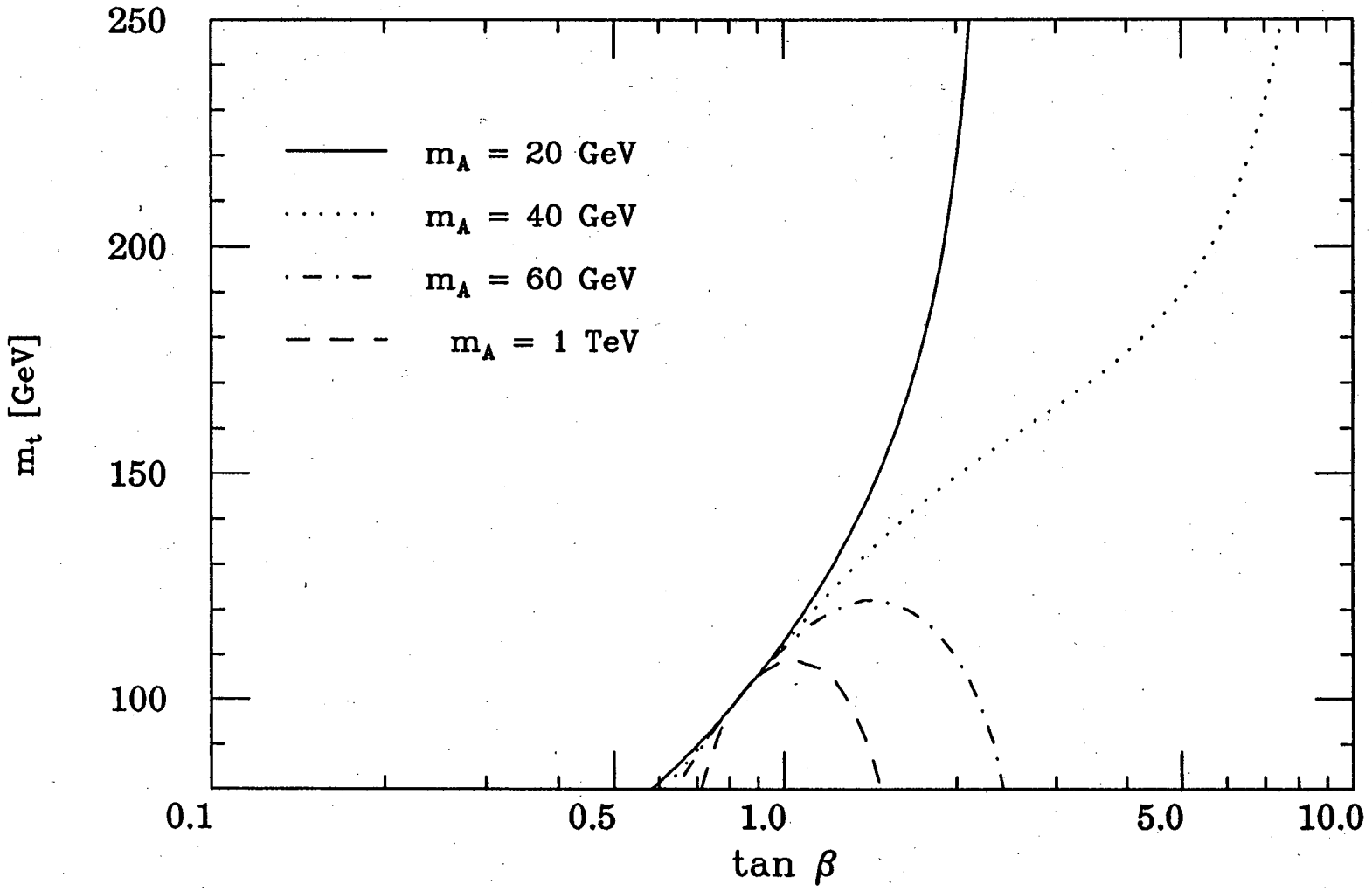
250
200
150
100
m_t [GeV]
m_A = 20 GeV
m_A = 40 GeV
m_A = 60 GeV
m_A = 1 TeV
0.1
0.5
1.0
5.0
10.0
tan β

Figure 3

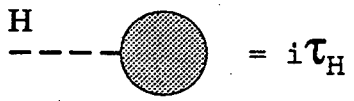

Figure 4

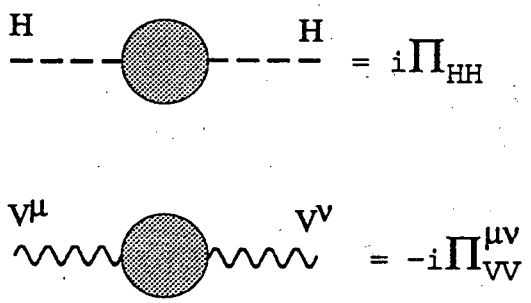

Figure 5

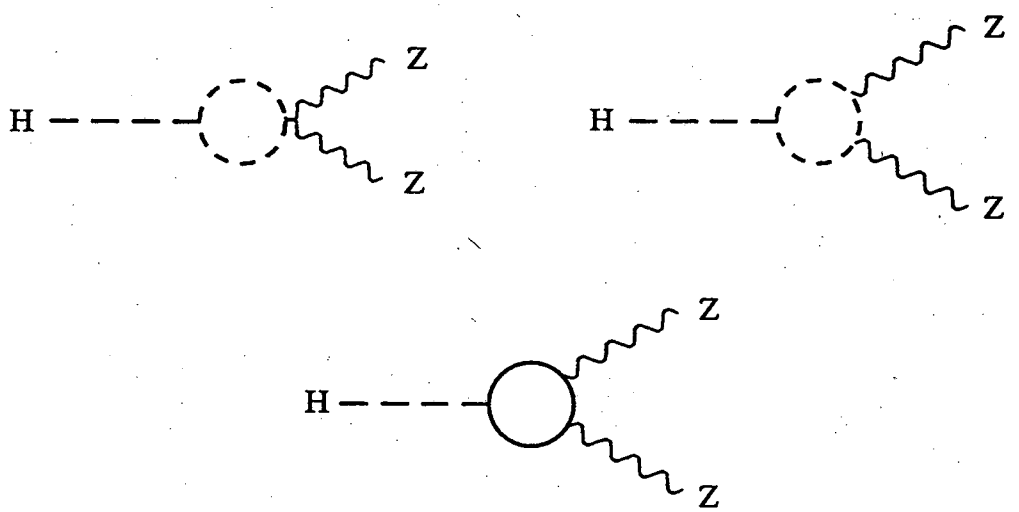

Figure 6

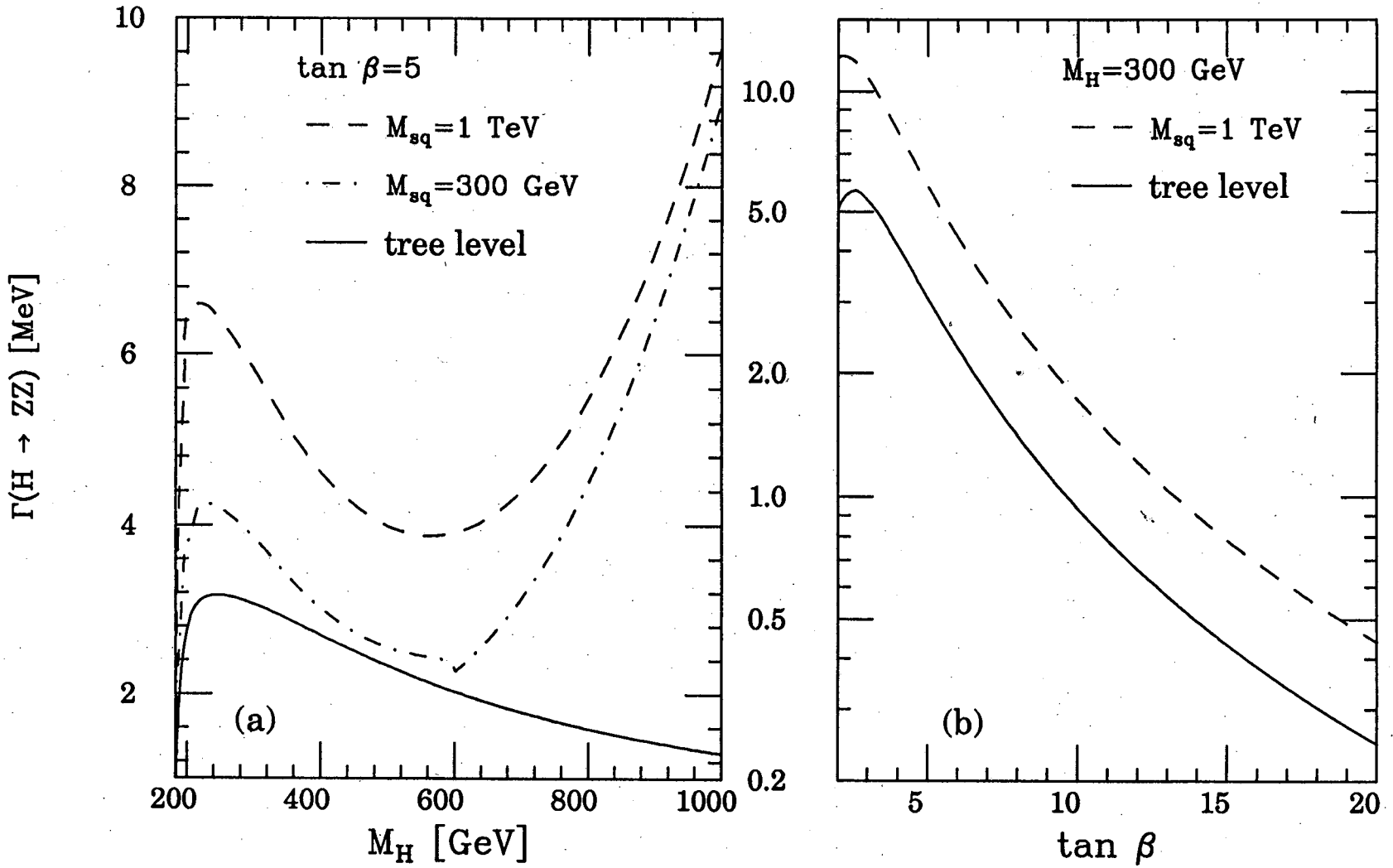
tan β=5
M_sq=1 TeV
M_sq=300 GeV
tree level
(a)
Γ(H → ZZ) [MeV]
M_H [GeV]
M_H=300 GeV
M_sq=1 TeV
tree level
(b)
tan β

Figure 7

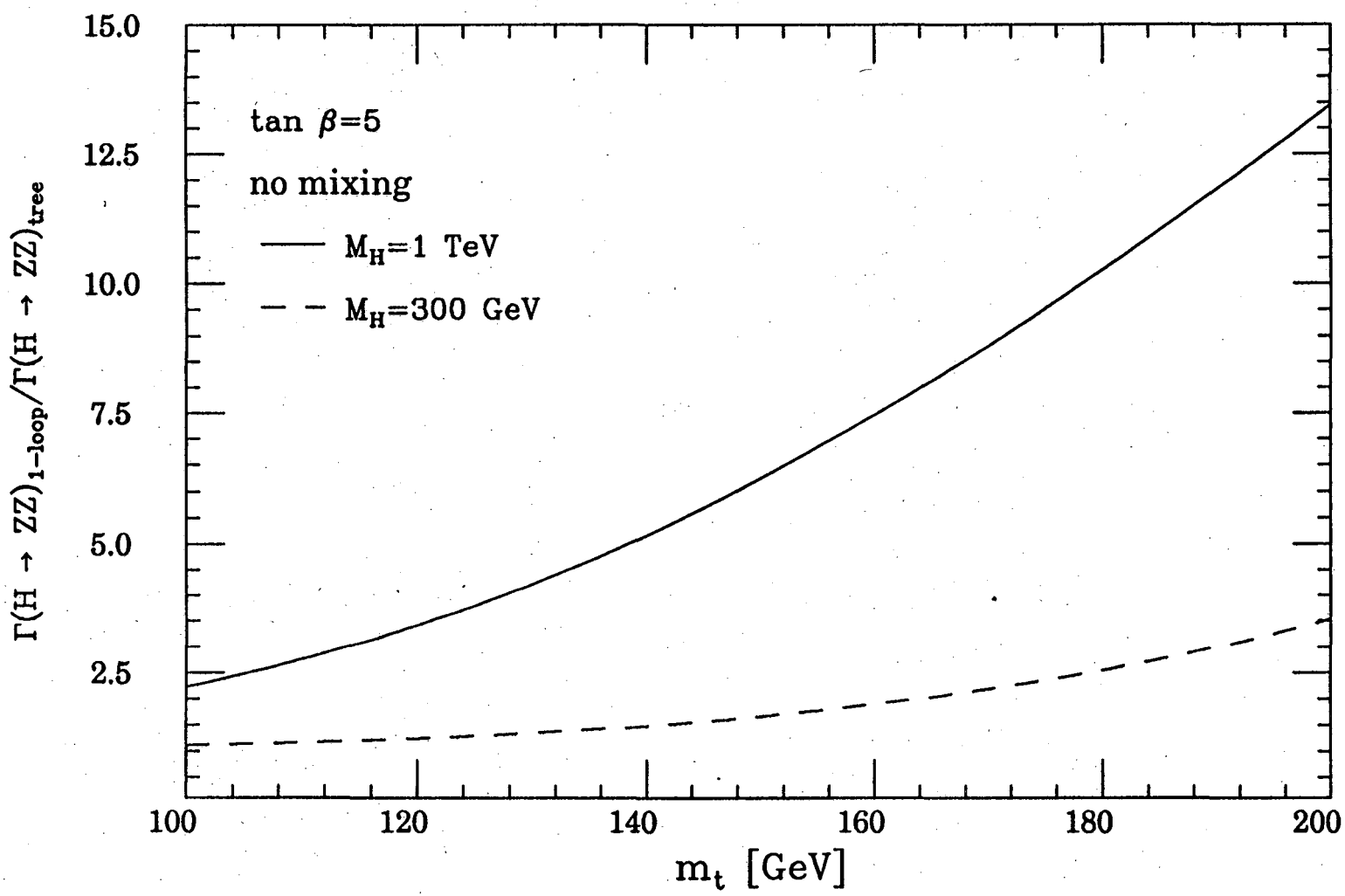
15.0
12.5
10.0
7.5
5.0
2.5
100
120
140
160
180
200
m_t [GeV]
$\Gamma(H \to ZZ)_{1-loop}/\Gamma(H \to ZZ)_{tree}$
tan β=5
no mixing
M_H=1 TeV
M_H=300 GeV

Figure 8

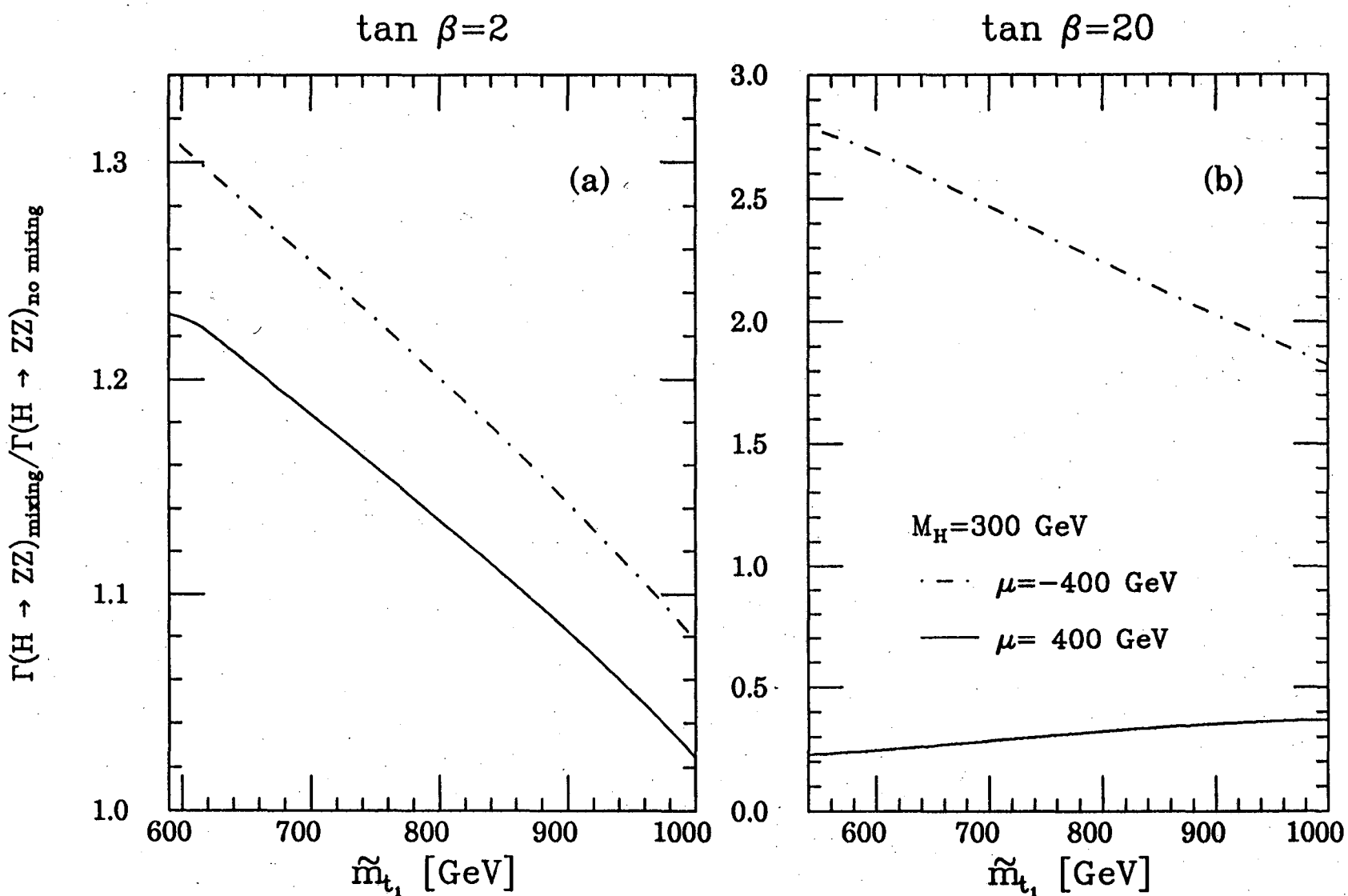
tan β=2
tan β=20
(a)
(b)
1.3
1.2
1.1
1.0
3.0
2.5
2.0
1.5
1.0
0.5
0.0
600
700
800
900
1000
Γ(H → ZZ)mixing/Γ(H → ZZ)no mixing
m̃t1 [GeV]
MH=300 GeV
μ=−400 GeV
μ= 400 GeV

Figure 9

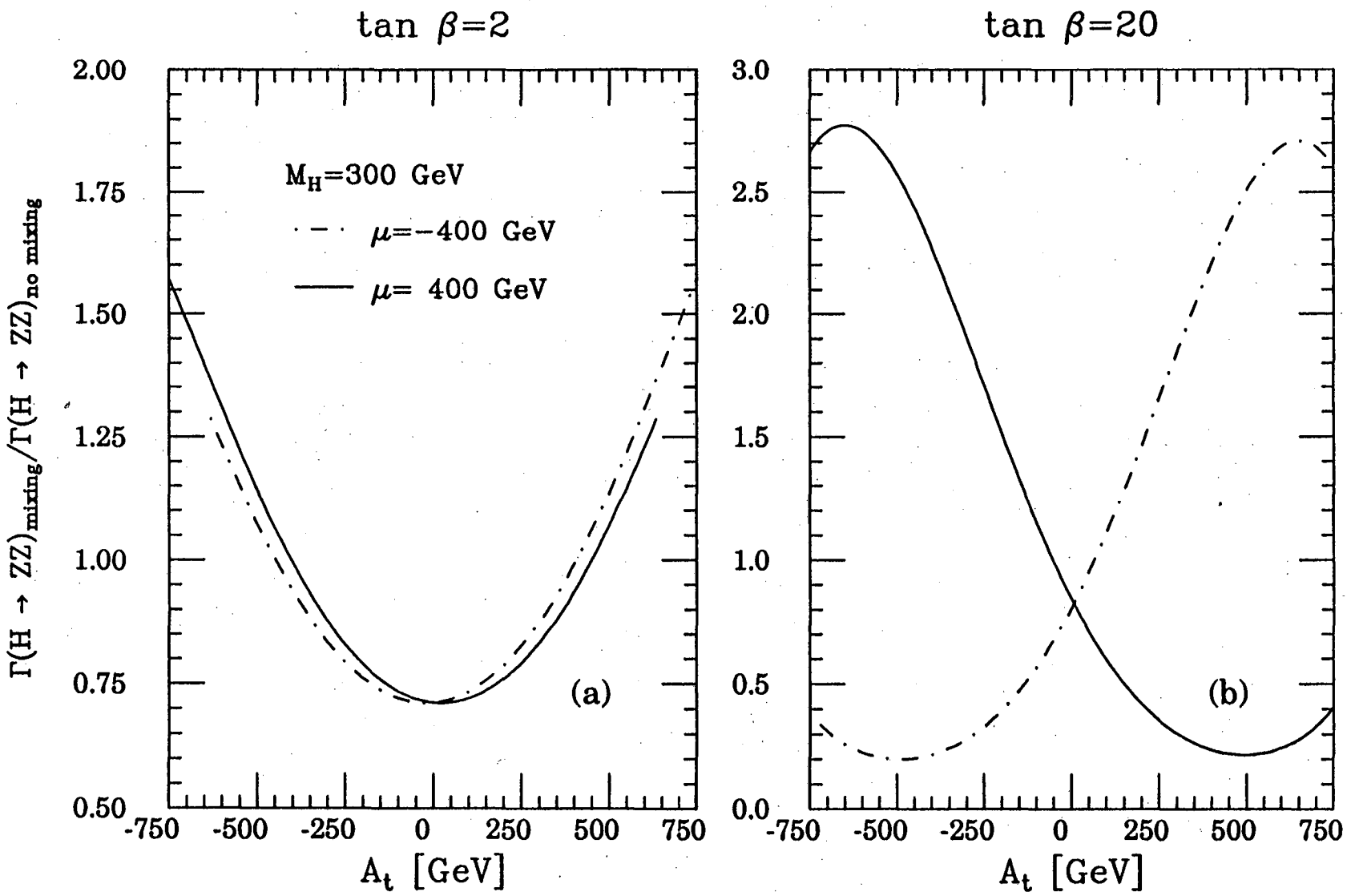
tan β=2
tan β=20
M_H=300 GeV
μ=−400 GeV
μ= 400 GeV
(a)
(b)
Γ(H → ZZ)_mixing/Γ(H → ZZ)_no mixing
A_t [GeV]
2.00
1.75
1.50
1.25
1.00
0.75
0.50
3.0
2.5
2.0
1.5
1.0
0.5
0.0
-750
-500
-250
0
250
500
750

Figure 10

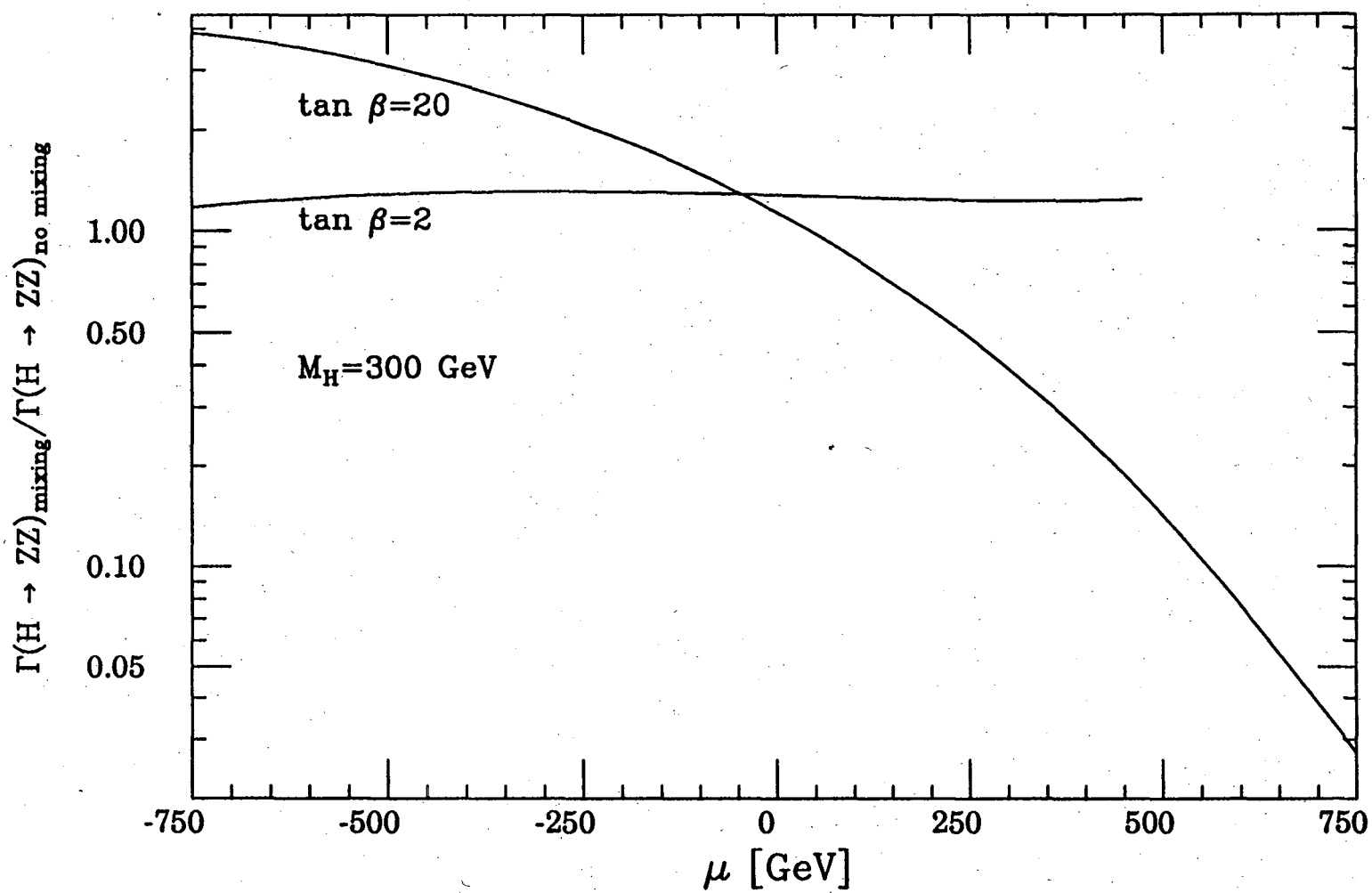
tan β=20
tan β=2
M_H=300 GeV
1.00
0.50
0.10
0.05
Γ(H → ZZ)_mixing/Γ(H → ZZ)_no mixing
-750
-500
-250
0
250
500
750
μ [GeV]

Figure 11

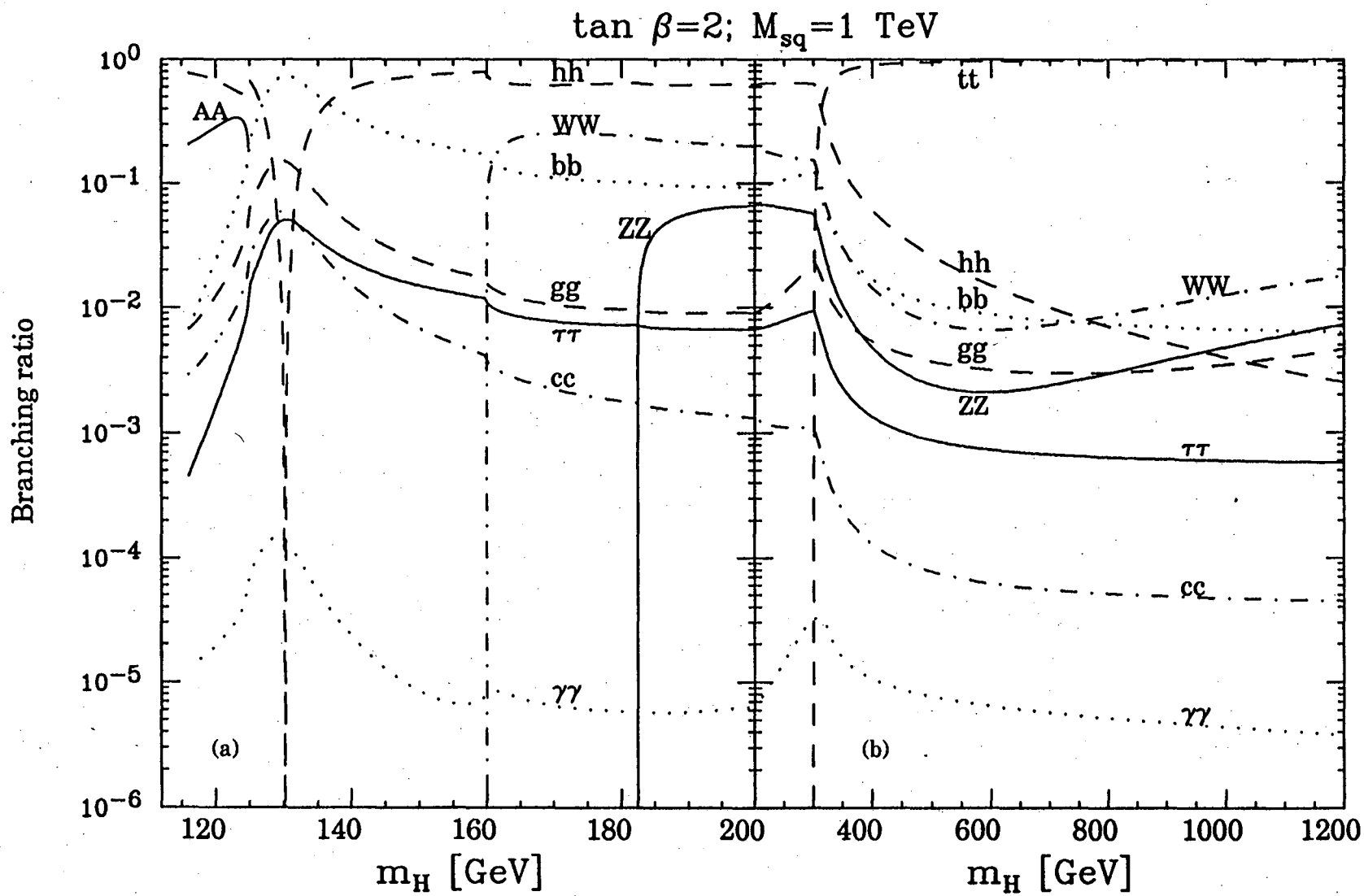
tan β=2; M_sq=1 TeV
Branching ratio
m_H [GeV]
m_H [GeV]
(a)
(b)
AA
hh
WW
bb
ZZ
gg
ττ
cc
γγ
tt
hh
bb
WW
gg
ZZ
ττ
cc
γγ

Figure 12

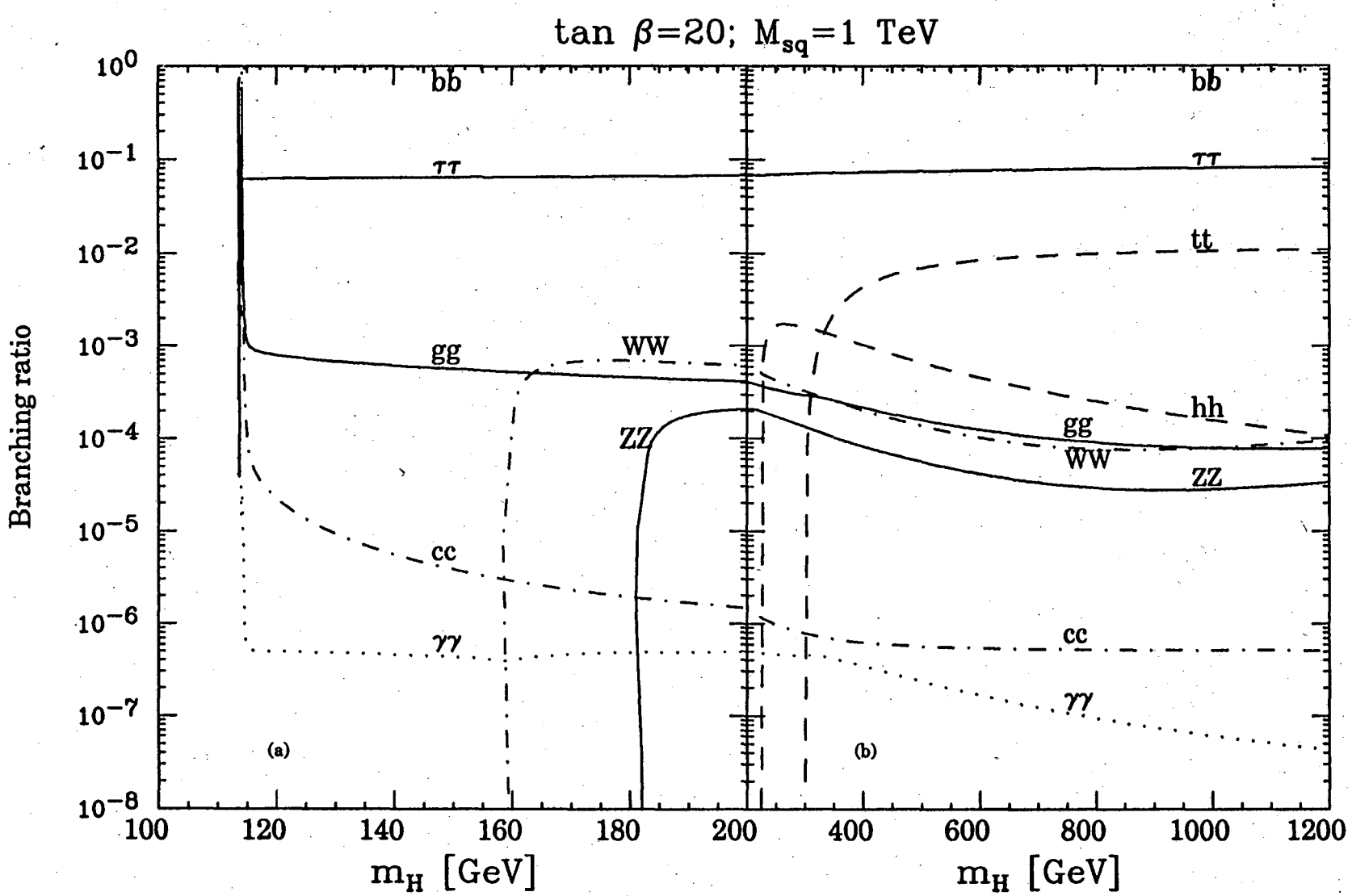
tan β=20; M_sq=1 TeV
Branching ratio
m_H [GeV]
m_H [GeV]
bb
ττ
gg
WW
ZZ
cc
γγ
tt
hh
(a)
(b)

Figure 13

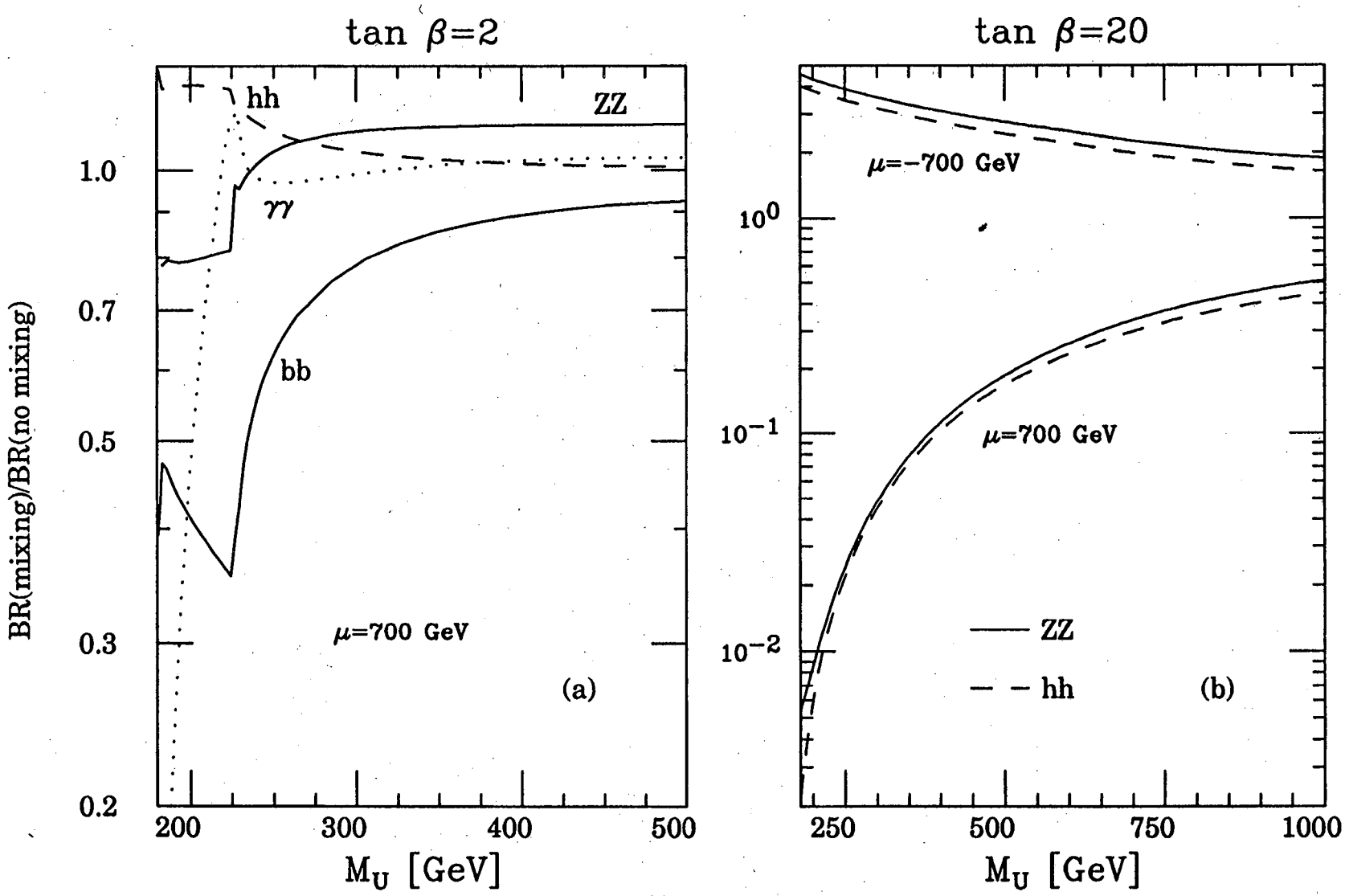
tan β=2
tan β=20
BR(mixing)/BR(no mixing)
1.0
0.7
0.5
0.3
0.2
hh
ZZ
γγ
bb
μ=700 GeV
(a)
200
300
400
500
M_U [GeV]
10^0
10^-1
10^-2
μ=-700 GeV
μ=700 GeV
ZZ
hh
(b)
250
500
750
1000
M_U [GeV]

Figure 14

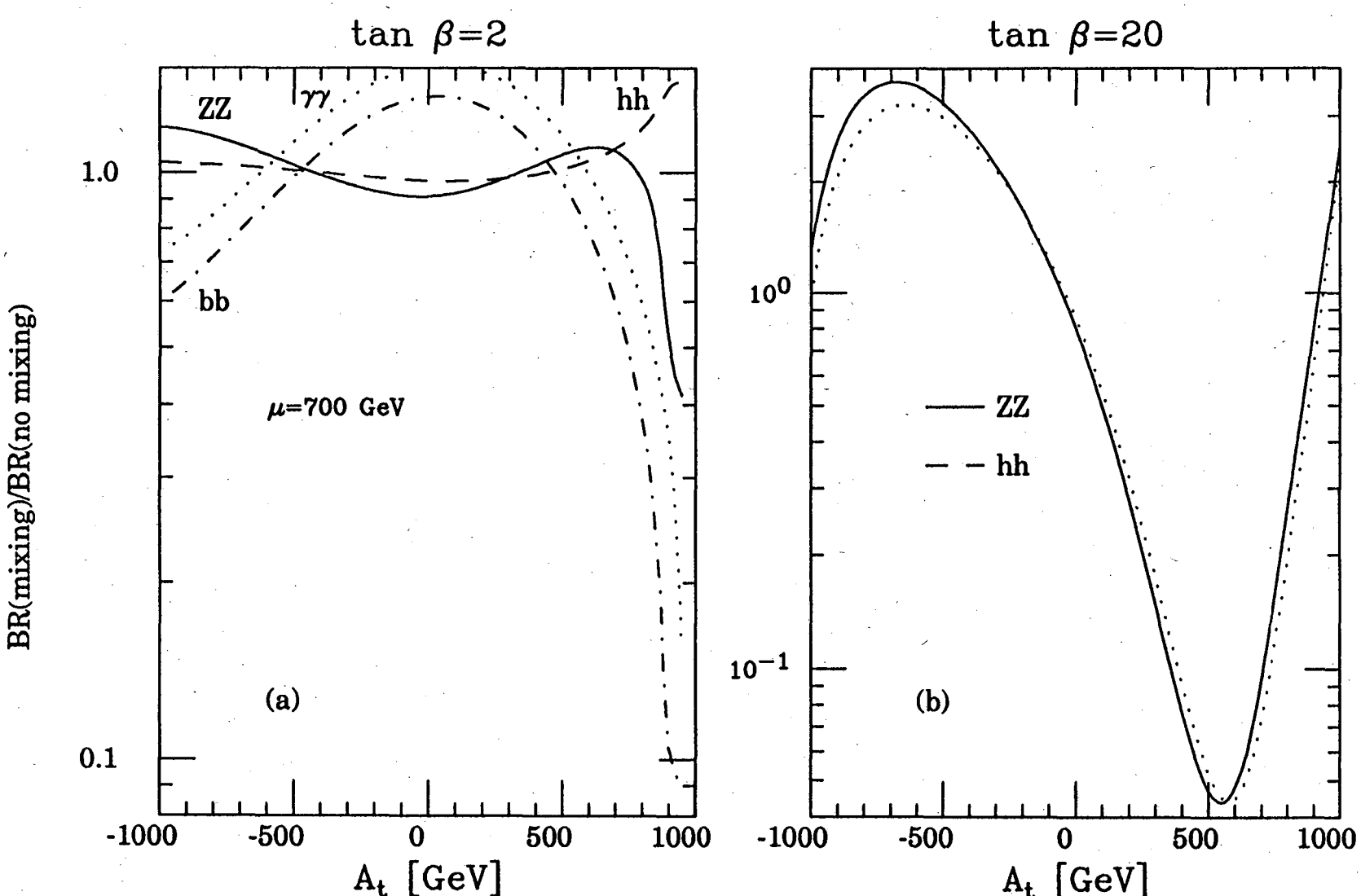
tan β=2
tan β=20
ZZ
γγ
hh
bb
μ=700 GeV
(a)
(b)
ZZ
hh
1.0
0.1
10^0
10^-1
-1000
-500
0
500
1000
A_t [GeV]
BR(mixing)/BR(no mixing)

Figure 15

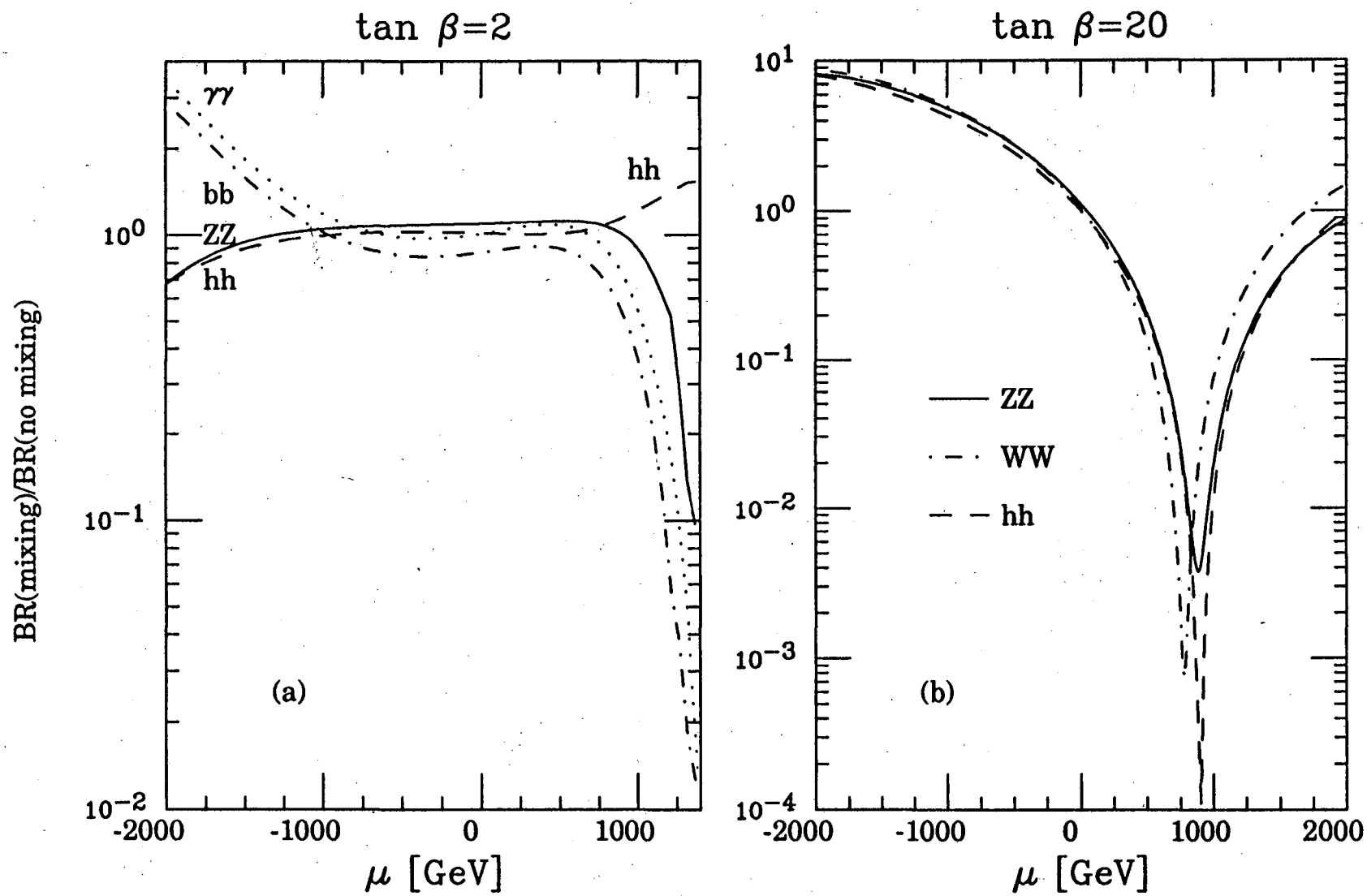
tan β=2
tan β=20
BR(mixing)/BR(no mixing)
γγ
bb
ZZ
hh
hh
(a)
(b)
ZZ
WW
hh
μ [GeV]
μ [GeV]

Figure 16

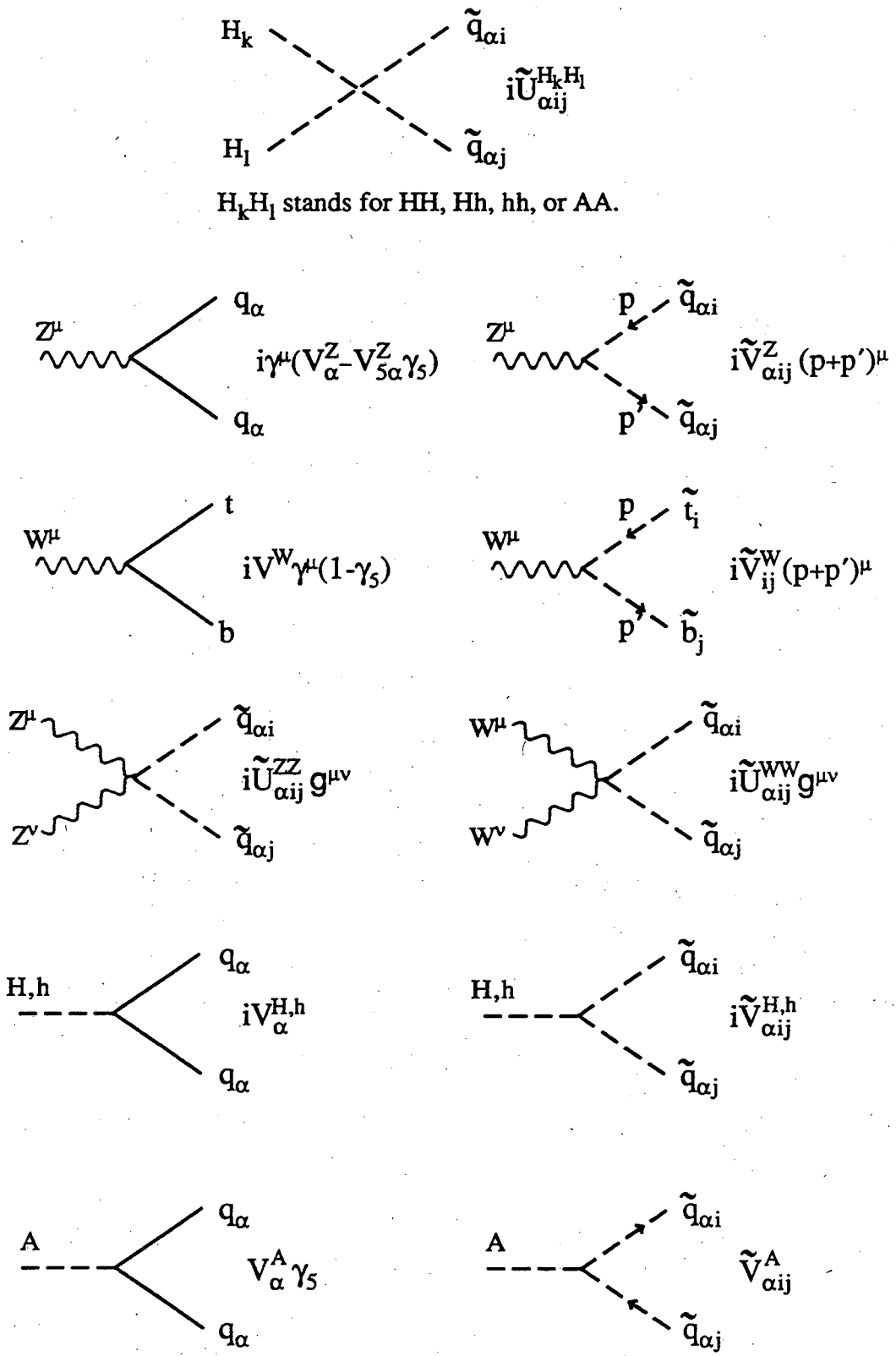
H_k
$\tilde{q}_{\alpha i}$
$i\tilde{U}^{H_k H_l}_{\alpha ij}$
H_l
$\tilde{q}_{\alpha j}$
$H_k H_l$ stands for HH, Hh, hh, or AA.
Z^μ
q_α
$i\gamma^\mu(V^Z_\alpha - V^Z_{5\alpha}\gamma_5)$
q_α
Z^μ
p
$\tilde{q}_{\alpha i}$
$i\tilde{V}^Z_{\alpha ij}(p+p')^\mu$
p'
$\tilde{q}_{\alpha j}$
W^μ
t
$iV^W\gamma^\mu(1-\gamma_5)$
b
W^μ
p
$\tilde{t}_i$
$i\tilde{V}^W_{ij}(p+p')^\mu$
p'
$\tilde{b}_j$
Z^μ
$\tilde{q}_{\alpha i}$
$i\tilde{U}^{ZZ}_{\alpha ij}g^{\mu\nu}$
Z^ν
$\tilde{q}_{\alpha j}$
W^μ
$\tilde{q}_{\alpha i}$
$i\tilde{U}^{WW}_{\alpha ij}g^{\mu\nu}$
W^ν
$\tilde{q}_{\alpha j}$
H,h
q_α
$iV^{H,h}_\alpha$
q_α
H,h
$\tilde{q}_{\alpha i}$
$i\tilde{V}^{H,h}_{\alpha ij}$
$\tilde{q}_{\alpha j}$
A
q_α
$V^A_\alpha\gamma_5$
q_α
A
$\tilde{q}_{\alpha i}$
$\tilde{V}^A_{\alpha ij}$
$\tilde{q}_{\alpha j}$

Figure 17

LAWRENCE BERKELEY LABORATORY
UNIVERSITY OF CALIFORNIA
TECHNICAL INFORMATION DEPARTMENT
BERKELEY, CALIFORNIA 94720